Figure 4 Enrichment of chromosomally deleted cells at the *HPRT1* locus. (A) Schematic illustration of the human *HPRT1* gene. The target sites of the *HPRT1*_B and *HPRT1*_E TALENs are shown by the yellow and red arrowheads, respectively. E, exon. (B) Flow cytometric analysis of HCT116 cells transfected with the *HPRT1*_B and *HPRT1*_E TALEN-encoding plasmids. Cells showing high expression (EGFP+/mCherry+) and minimal expression (EGFP−/mCherry−) were collected (squares). Indexes of numbers and percentages of collected cells are listed in Table S5 in Supporting Information. Vertical and horizontal lines indicate background fluorescence levels of EGFP and mCherry, respectively. (C) Cel-I assays of cells transfected with the *HPRT1_B* and *HPRT1*_E TALEN-encoding separate vectors (Ligation−) and single vectors (Ligation+). The arrowheads indicate the expected positions of the digested products.% NHEJ (nonhomologous end-joining) was estimated using ImageJ software as previously described (Hansen *et al.* 2012). (D) Genomic RCR analysis of chromosomal deletions at the *HPRT1* locus of unselected, EGFP−/mCherry−, and EGFP+/mCherry+ cells transfected with the *HPRT1*_B and *HPRT1*_E TALEN-encoding plasmids and untransfected control cells. The arrowhead indicates the expected position of the PCR product with the 1100-bp deleted sequence. (E, F) Frequencies of chromosomal deletions in unselected (E) and EGFP+/mCherry+ (F) cells. The genomic PCR products were subcloned, and colony PCR was carried out. After analysis by agarose gel electrophoresis, the nucleotide sequences of the smaller DNA fragments were determined. Red clone numbers indicate the sequenced clones. The wild-type sequence of *HPRT1* is shown at the top with the TALEN target sequence (capital letters with underlines). Deletions are indicated by dashes.

expression vectors using the mismatch-sensitive endonuclease (Cel-I) assay (Fig. 4C). The results showed that the mutagenic frequencies of the unified TALEN vectors were at similar levels to those of the separate TALEN expression vectors.

To enrich cells with large deletions, we simultaneously transfected the unified expression vectors for the *HPRT1*_B and *HPRT1*_E TALEN pair-expressing plasmids into HCT116 cells. At 72 h post-transfection, we obtained unselected, EGFP−/mCherry− and EGFP+/mCherry+ cells and amplified the DNA fragments including the *HPRT1*_B and *HPRT1*_E TALEN target sites by PCR using genomic DNA extracted from these cells as well as negative control cells (Fig. 4B, squares; Fig. 4D). We clearly observed 1100-bp deleted DNA fragments in the PCR products of EGFP+/mCherry+ cells and weakly detected such fragments in the products of transfected-unselected cells, but did not detect such fragments in the products of untransfected-unselected cells and EGFP−/mCherry− cells. To investigate whether the smaller DNA fragments were caused by chromosomal deletions, the DNA fragments amplified by PCR using genomic DNA extracted from unselected cells were subcloned, and the nucleotide sequences of the smaller DNA fragments were determined (Fig. 4E). As a result, we found that the left site of the *HPRT1*_E TALENs and right site of the *HPRT1*_B TALENs were joined and that a region of approximately 1100 bp in length of the genomic sequence between the two TALEN sites was deleted. The frequency of chromosomal deletions was 3% in unselected cells. In addition, large deletions were observed in the DNA fragments of EGFP+/mCherry+ cells by sequencing, and the frequency of these large deletions was 41%, showing 13.7-fold enrichment of deleted cells after the selection (Fig. 4F).

Next, we investigated whether this system enables the enrichment of cells with large deletions in an autosomal genomic locus. We constructed two pairs of TALENs targeting the *ATM* locus using the FUSE method, in which the *ATM*_A TALEN target site was located approximately 1400-bp downstream of the *ATM*_D TALEN target site (Fig. 5A). After confirmation of the TALEN activities by the SSA assay, we examined the formation of short indels (Fig. 5C) and large deletions (Fig. 5D) with or without fluorescence selection (Fig. 5B). We subsequently analyzed the deletion frequencies in transfected cells by DNA sequencing. For the *ATM* locus, the frequencies of chromosomal deletions were 11% (Fig. 5E) and 77% (Fig. 5F) in unselected and EGFP+/mCherry+ cells, respectively, indicating 7-fold enrichment of cells with large deletions after the selection (Table 1).

Enrichment of cells with TALEN-induced extra-large chromosomal deletions

To test the ability of our FUSE method and FAST-id system to enrich cells with more complex chromosomal rearrangements, we finally tried enrichment of cells with extra-large chromosomal deletions, chromosomal inversions and translocations. We additionally constructed a pair of TALEN targeting nuclear protein, ataxia–telangiectasia locus (*NPAT*) gene (*NPAT*_A TALEN, Fig. 6A), whose target site is approximately 30 kb away from *ATM*_A TALEN target site. After confirming the mutagenic activity of FUSEd and unFUSEd *NPAT*_A TALENs by Cel-I assay (Fig. 6C), we transfected *NPAT*_A and *ATM*_A TALEN

© 2014 The Authors
Genes to Cells © 2014 by the Molecular Biology Society of Japan and Wiley Publishing Asia Pty Ltd

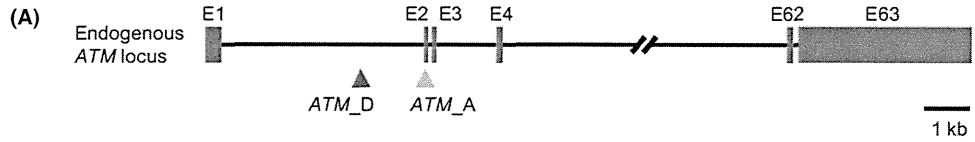

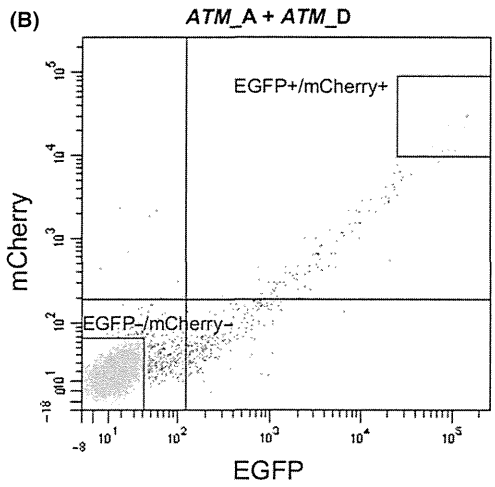

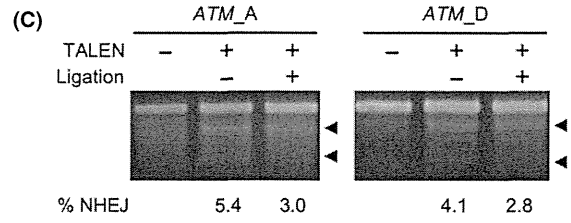

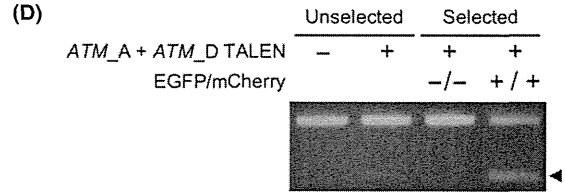

(E) *ATM*_A + *ATM*_D TALEN (Unselected cells)

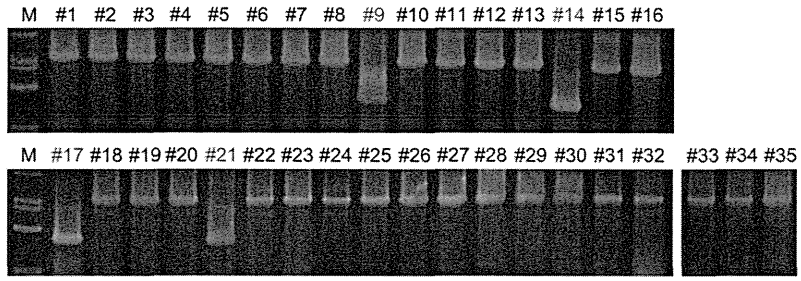

ATM_A + ATM_D Unselected cells 11%(4/35)

*ATM*_D TALEN Left site — *ATM*_A TALEN Right site

```
gaggcttggtGTACGAATGATCCTGTCactcaggtagtgagc..1390bp..tgcttatctgctgccGTCAACTAGAACATGATagagctacag WT
gaggcttggtGTACGAATGATCCTGTCacgg----------tgccGTCAACTAGAACATGATagagctacag x2
gaggcttggtGTACGAATGATCCTGTCac----------tgccGTCAACTAGAACATGATagagctacag x2
```

(F) *ATM*_A + *ATM*_D TALEN (EGFP+/mCherry+ cells)

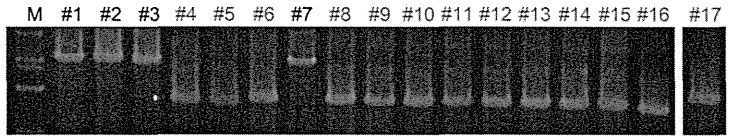

ATM_A + ATM_D EGFP+/mCherry+ cells 77%(13/17)

*ATM*_D TALEN Left site — *ATM*_A TALEN Right site

```
gaggcttggtGTACGAATGATCCTGTCactcaggtagtgagc..1390bp..tgcttatctgctgccGTCAACTAGAACATGATagagctacag WT
gag----------ctacag x2
gaggcttggtGTACGAATGATCCTGTCactcaggttag----------tgctgccGTCAACTAGAACATGATagagctacag
gaggcttggtGTACGAATGATCCTGTCactctgct----------gccGTCAACTAGAACATGATagagctacag
gaggcttggtGTACGAATGATCCTGTCactcag----------ccGTCAACTAGAACATGATagagctacag
gaggcttggtG-------GATCaT----------ctgccGTCAACTAGAACATGATagagctacag
gaggcttggtGTACGAATGATCCTGTCactcaggttg----------gctgccGTCAACTAGAACATGATagagctacag
gaggcttggtGTACGAATGATCCTGTCactc----------tgccGTCAACTAGAACATGATagagctacag
gaggcttggtGTACGAATGATCCTGTCactcagg----------cGTCAACTAGAACATGATagagctacag
gaggcttggtGTACGAATGATCCTGTCa----------tgccGTCAACTAGAACATGATagagctacag
gaggcttggtGTACGAATGATCCTGTCactcaggtagt----------ctgccGTCAACTAGAACATGATagagctacag
gaggcttggtGTACGAATGATCCTGTCactcaggtagt----------AACTAGAACATGATagagctacag
gaggcttggtGTACGAATGATCCTGTCactcaggtaat----------gctgccGTCAACTAGAACATGATagagctacag
```


© 2014 The Authors
Genes to Cells © 2014 by the Molecular Biology Society of Japan and Wiley Publishing Asia Pty Ltd

Figure 5 Enrichment of chromosomally deleted cells at the *ATM* locus. (A) Schematic illustration of the human *ATM* gene. The target sites of the *ATM*_A and *ATM*_D TALENs are shown by the yellow and red arrowheads, respectively. E, exon. (B) Flow cytometric analysis of HCT116 cells transfected with the *ATM*_A and *ATM*_D TALEN-encoding plasmids. Cells showing high expression (EGFP+/mCherry+) and minimal expression (EGFP−/mCherry−) were collected (squares). Indexes of numbers and percentages of collected cells are listed in Table S5 in Supporting Information. Vertical and horizontal lines indicate background fluorescence levels of EGFP and mCherry, respectively. (C) Cel-I assays of cells transfected with the *ATM*_A and *ATM*_D TALEN-encoding separate vectors (Ligation−) and single vectors (Ligation+). The arrowheads indicate the expected positions of the digested products.% NHEJ (nonhomologous end-joining) was estimated using ImageJ software as previously described (Hansen *et al.* 2012). (D) Genomic RCR analysis of chromosomal deletions at the *ATM* locus of unselected, EGFP−/mCherry−, or EGFP+/mCherry+ cells transfected with the *ATM*_A and *ATM*_D TALEN-encoding plasmids and untransfected control cells. The arrowhead indicates the expected position of the PCR product with the 1400-bp deleted sequence. (E, F) Frequencies of chromosomal deletions in unselected (E) and EGFP+/mCherry+ (F) cells. The genomic PCR products were subcloned and colony PCR was carried out. After analysis by agarose gel electrophoresis, the nucleotide sequences of the smaller DNA fragments were determined. Red clone numbers indicate the sequenced clones. The wild-type sequence of *ATM* is shown at the top with the TALEN target sequence (capital letters with underlines). Deletions are indicated by dashes.

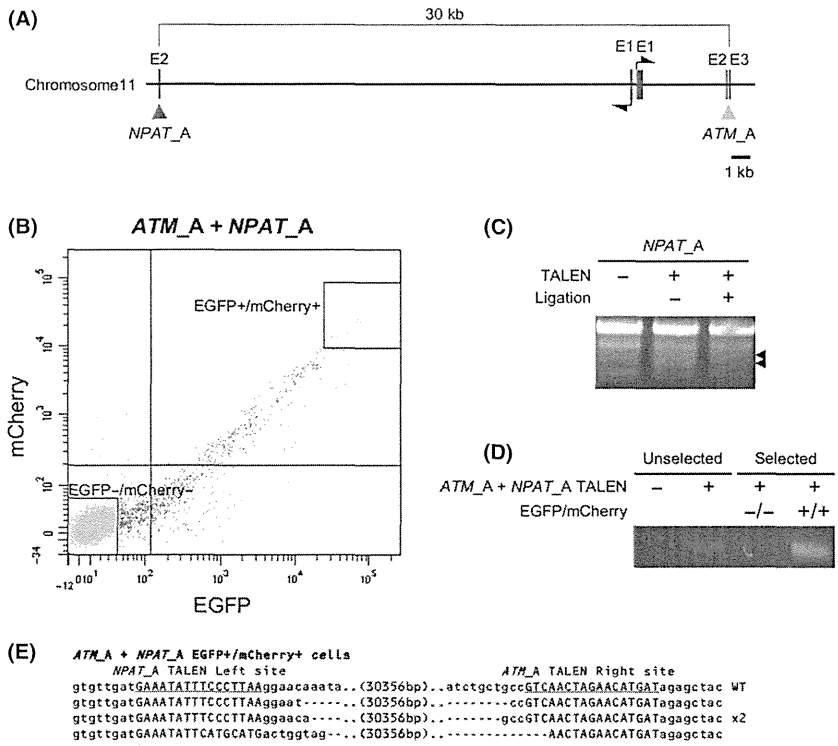

Figure 6 Enrichment of cells with extra-large chromosomal deletions. (A) Schematic illustration of a part of human chromosome 11. The target sites of *ATM*_A and *NPAT*_A TALENs are shown by the yellow and red arrowheads, respectively. E, exon. (B) Flow cytometric analysis of HCT116 cells transfected with *ATM*_A and *NPAT*_A TALEN-encoding plasmids. Cells showing high expression (EGFP+/mCherry+) and minimal expression (EGFP−/mCherry−) were collected (squares). Indexes of numbers and percentages of collected cells are listed in Table S5 in Supporting Information. Vertical and horizontal lines indicate background fluorescence levels of EGFP and mCherry, respectively. (C) Cel-I assay of the cells transfected with *NPAT*_A TALEN-encoding separate vectors (Ligation-) and a single vector (Ligation+). The arrowheads indicate the expected positions of the digested products. (D) Genomic RCR analysis of extra chromosomal deletions at the chromosome 11 of unselected, EGFP−/mCherry−, or EGFP+/mCherry+ cells transfected with *ATM*_A and *NPAT*_A TALEN-encoding plasmids and untransfected control cells. (E) Sequences observed in EGFP+/mCherry+ cells transfected with *ATM*_A and *NPAT*_A TALEN-encoding plasmids. The wild-type sequence of a part of chromosome 11 is shown at the top with the TALEN target sequence (capital letters with underlines). Deletions are indicated by dashes.

© 2014 The Authors
Genes to Cells © 2014 by the Molecular Biology Society of Japan and Wiley Publishing Asia Pty Ltd

pair-expressing plasmids into HCT116 cells. Genomic PCR and DNA sequencing showed that cells with 30-kb chromosomal deletions were successfully enriched by FACS selection (Fig. 6B,D,E).

It has been reported that chromosomal inversion sometimes occurs with the use of two pairs of TALENs targeting the same chromosome (Lee *et al.* 2012; Gupta *et al.* 2013; Xiao *et al.* 2013). Therefore, we carried out PCR analyses to investigate whether chromosomal inversions were generated. For *HPRT1*, one of the ten sequences (Fig. 4F, #7 among the black-lettered numbers) exhibited chromosomal inversion with an expected size in EGFP+/mCherry+ cells transfected with the *HPRT1*_B and *HPRT1*_E TALEN pair expression vectors. However, no chromosomal inversions were detected in 35 sequences (Fig. 4E, all black-lettered numbers) with the expected size in unselected cells transfected with the *HPRT1*_B and *HPRT1*_E TALEN expression vectors. On the other hand, chromosomal inversions were not detected in cells transfected with the *ATM*_A and *ATM*_D TALEN expression vectors.

Double-strand breaks induced on different chromosomes potentially cause chromosomal translocations (Brunet *et al.* 2009; Piganeau *et al.* 2013). We transfected *ATM*_A and *HPRT1*_E TALEN pair-expressing plasmids into HCT116 cells, collected EGFP+/mCherry+ cells, and tried to detect translocated alleles by genomic PCR analysis, but no intended amplicons appeared.

Discussion

In this study, we have showed that our FAST-id system enabled enrichment of cells with TALEN-induced mutations and that the combination of the FAST-id system and FUSE method efficiently enriched cells with TALEN-induced large deletions.

The FAST-id system and FUSE method have several advantages compared with conventional methods using additional reporter vectors. First, we construct a bicistronic expression vector that is expected to express the same number of TALEN and fluorescent protein molecules, meaning that there is no necessity to construct and transfect additional plasmids. Furthermore, transfection of the vector enables us to exactly identify the cells expressing the TALEN and evaluate the expression level of the TALEN by monitoring the expression level of the fluorescent protein. Second, the FUSE method enables us to construct vectors that express the same molecular number of left TALEN, right TALEN, and fluorescent protein, and thus, the combination of the FAST-id system and FUSE method enables us to select cells expressing both the left and right TALENs by monitoring the fluorescent protein. Third, our system enables us to reduce the kinds of vectors required for transfection, which is expected to improve the selection efficiency for cells with mutations. In fact, the mutation rates of TALEN-transfected cells after selection in this study (83% and 100%) were higher than those in previous studies (Kim *et al.* 2011, 2013a). Moreover, our methods are thought to be capable of enriching cells with TALEN-induced mutations and large deletions after synthesized mRNA transfection, whereas DNA transfection, which has a risk of random integration into the genome, is indispensable for previous reporter vector-based methods. Fourth, our system is easy to use, because the novel vectors for the FAST-id system and FUSE method are fully compatible with the Golden Gate TALEN and TAL Effector Kit (Cermak *et al.* 2011) and the Yamamoto Laboratory TALEN Construction and Evaluation Accessory Pack (Sakuma *et al.* 2013) distributed by Addgene (Cambridge, MA, USA).

Transcription activator-like effector nuclease-mediated large deletion is a useful technique for analyzing the functions of not only a single gene, but also multiple genes. In zebrafish, it has been reported that a noncoding RNA gene cluster was successfully excised from the genome using two pairs of TALENs (Liu *et al.* 2013). In that case, the excised genomic region was approximately 1.2 kb in length, which was a similar size to the experiments in the present study. Furthermore, it has been shown that much larger genomic regions, up to megabases in length, can be deleted through the use of two pairs of TALENs in zebrafish (Gupta *et al.* 2013) and cultured cells (Kim *et al.* 2013b). Although a previous report estimated quite low frequencies of TALEN-mediated large chromosomal deletions (0.61% for 3.6-Mb deletion and 0.40% for 24-Mb deletion; Kim *et al.* 2013b), our FAST-id system and FUSE method have the possibility of enriching cells with such large chromosomal deletions, thereby enabling the disruption of multiple genes including clustered genes that have redundant functions and disease-related genes that are known to cause afflictions such as cancer and neuropsychiatric disorders through copy number variations.

As all the TALENs used in this study contain homodimeric FokI nuclease domains, there remains to be improved regarding targeting specificity. It is expected that TALENs containing obligate heterodimeric FokI nuclease domains will significantly

© 2014 The Authors
Genes to Cells © 2014 by the Molecular Biology Society of Japan and Wiley Publishing Asia Pty Ltd

decrease the risk of off-target mutations, especially in the experiments using two pairs of TALENs.

In conclusion, our system is simple, easy, and reliable for the enrichment of cells with TALEN-induced mutations or large deletions. To the best of our knowledge, this is the first report of efficient enrichment of cells with TALEN-induced chromosomal deletions. Importantly, we successfully showed not only approximately 1-kb deletions but also 30-kb extra-large chromosomal deletions. Our system will promote the utility of TALENs in both basic and biomedical research.

Experimental procedures

Construction of co-expression vectors for TALENs and fluorescent proteins

The pcDNA-mC-2A-TAL-NC2 plasmid, a destination vector for construction of the mCherry-2A-TALEN expression plasmid, was constructed by the In-Fusion cloning method (Clontech, Mountain View, CA, USA). Briefly, the mCherry sequence was amplified by PCR using mCherry-F and mCherry-2A-R primers (Table S1 in Supporting Information). 2A sequences were synthesized and converted to double-stranded DNA by primer extension using 2A-F and 2A-R oligonucleotides (Table S1 in Supporting Information). pcDNA-TAL-NC2 plasmids (Addgene) were linearized by inverse PCR using pcDNA-TAL-NC-Inverse-F and pcDNA-TAL-NC-Inverse-R primers (Table S1 in Supporting Information). These three DNA fragments were assembled by the In-Fusion cloning method. As the products generated by In-Fusion cloning erroneously contained a stop codon in the mCherry sequence, it was excluded by inverse PCR using 2A-Inverse-F and mCherry-Inverse-R primers (Table S1 in Supporting Information) to generate pcDNA-mC-2A-TAL-NC2 plasmids. The pcDNA-eG-2A-TAL-NC2 plasmid, a destination vector for construction of the EGFP-2A-TALEN expression plasmid, was constructed by the In-Fusion cloning method. Briefly, pcDNA-mC-2A-TAL-NC2 plasmids were linearized, and the mCherry sequence was excluded using pcDNA-TAL-NC-2A-Inverse-F and pcDNA-TAL-NC-Inverse-R primers (Table S1 in Supporting Information). The EGFP sequence was amplified by PCR using Infusion-EGFP-F and Infusion-EGFP-R primers (Table S1 in Supporting Information). These two DNA fragments were assembled by the In-Fusion cloning method. For unification of one TALEN pair into a single vector, pcDNA-mC-2A-TAL-NC2-Uni, pcDNA-eG-2A-TAL-NC2-Uni, and pcDNA-2A-TAL-NC2-Uni plasmids were constructed as destination vectors for construction of mCherry-2A-TALEN-(BamHI), EGFP-2A-TALEN-(BamHI), and (BamHI)-2A-TALEN expression vectors, respectively. The pcDNA-mC-2A-TAL-NC2-Uni and pcDNA-eG-2A-TAL-NC2-Uni plasmids were constructed by inverse PCR using +BamHI-FokI-F and +BamHI-FokI-R primers (Table S1 in Supporting Information) for insertion of a BamHI site (5′-GGATCC-3′). The pcDNA-2A-TAL-NC2-Uni plasmid was constructed by inverse PCR from the pcDNA-mC-2A-TAL-NC2 plasmid using +ATG + BamHI-2A-F and pcDNA-TAL-NC-Inverse-R primers (Table S1 in Supporting Information) to exclude the mCherry sequence and insert a start codon and BamHI site (5′-ATGGGATCC-3′).

Design and construction of TALENs

The design of the *HPRT1*_B TALENs was described previously (Sakuma *et al.* 2013). *HPRT1*_E, *ATM*_A, and *ATM*_D TALENs were newly designed using TAL Effector Nucleotide Targeter 2.0 (Doyle *et al.* 2012; https://tale-nt.cac.cornell.edu/node/add/talen-old). The target sites of each TALEN are listed in Table S2, in Supporting Information (capital letters). The TALENs were constructed as previously described (Sakuma *et al.* 2013) using the modified destination vectors described above. The combinations of the TALEN arrays and vectors used are listed in Table S3 in Supporting Information. The left and right TALEN arrays of one TALEN pair were unified into a single vector by double restriction enzyme digestion using BamHI (Takara Bio, Shiga, Japan) and PvuI (TaKaRa Bio) and subsequent ligation. Successful construction of one TALEN pair into a single vector was confirmed by digestion with XbaI (Takara Bio). Because the vector contained XbaI sites exclusively in the N-terminal domains of the TALENs, an approximately 3-kb DNA fragment appeared after XbaI digestion if the two TALEN vectors were assembled successfully.

Transfection and Cel-I assay

Transfection for the Cel-I assay was carried out as follows. On the day before transfection, 200 000 HCT116 cells were plated into 35-mm dishes. On the day of transfection, a total of 2.5 μg of TALEN plasmids was transfected using 5.0 μL of Lipofectamine LTX (Invitrogen, Carlsbad, CA, USA) and 2.0 μL of Plus Reagent (Invitrogen) according to the manufacturer's instructions. On the day after transfection, the cells were moved to 60-mm dishes. At 72 h post-transfection, the cells were collected and their genomic DNA was isolated using a DNeasy Blood & Tissue Kit (Qiagen, Hilden, Germany). Genomic PCR was carried out with the primers listed in Table S4 in Supporting Information. The amplified products were purified with a Wizard SV Gel and PCR Clean-Up System (Promega, Madison, WI, USA), and 400 ng of purified DNA was used for the Cel-I assay with a SURVEYOR Mutation Detection Kit (Transgenomic, Omaha, NE, USA) according to the manufacturer's instructions. The products were analyzed by electrophoresis in 3% agarose gels and ethidium bromide staining.

Transfection and FACS

Transfection for cell sorting was carried out as described above with several modifications. On the day before transfection,

© 2014 The Authors
Genes to Cells © 2014 by the Molecular Biology Society of Japan and Wiley Publishing Asia Pty Ltd

1 500 000 HCT116 cells were plated into 60-mm dishes. On the day of transfection, a total of 6.0 μg of TALEN plasmids was transfected using 15 μL of Lipofectamine LTX (Invitrogen) and 6.0 μL of Plus Reagent (Invitrogen) according to the manufacturer's instructions. On the day after transfection, the cells were moved to 100-mm dishes. At 72 h post-transfection, the cells were analyzed and sorted using a FACSAria II (BD Biosciences, San Jose, CA, USA). Cells with weak or strong EGFP and mCherry signals, EGFP−/mCherry− cells and EGFP+/mCherry+ cells, respectively, were sorted for each TALEN-transfected sample. Untransfected cells were used as negative controls.

Analysis of mutations in cells transfected with TALENs

Twenty thousand EGFP−/mCherry−, EGFP+/mCherry+, unselected, and control cells were collected, and their genomic DNA was isolated with a DNeasy Blood & Tissue Kit (Qiagen). Genomic PCR was carried out with the primers listed in Table S4 in Supporting Information. The amplified products were purified with a Wizard SV Gel and PCR Clean-Up System (Promega), and 200 ng of purified DNA was digested with Hpy188I (New England Biolabs, Ipswich, MA, USA) or Fnu4HI (New England Biolabs) for the RFLP analyses. The products were analyzed by electrophoresis in 3% agarose gels and ethidium bromide staining. For DNA sequencing analyses, the PCR products amplified from genomic DNA from unselected cells or EGFP+/mCherry+ cells were subcloned into pCR2.1/TOPO (Life Technologies, Carlsbad, CA, USA), and the nucleotide sequences were determined from colony PCR products using a CEQ 8000 Genetic Analysis System (Beckman Coulter, Brea, CA, USA).

For large deletion experiments, cell collection, genomic DNA extraction, genomic PCR, and sequence determination were carried out as described above with slight modifications. The amplified products were directly analyzed by electrophoresis in 1% agarose gels and ethidium bromide staining without restriction enzyme digestion. Detection of extra-large deletions was carried out by PCR using Cel-I-NPAT_A-F and Cel-I-ATM_A-R primers (Table 4 in Supporting Information) for cells transfected with *NPAT*_A and *ATM*_A TALEN-encoding plasmids. Detection of chromosomal inversions was carried out by PCR using Cel-I-HPRT1_B-F and Cel-I-HPRT1_E-F primers (Table S4 in Supporting Information) for cells transfected with the *HPRT1*_B and *HPRT1*_E TALEN-encoding plasmids. For cells transfected with the *ATM*_A and *ATM*_D TALEN-encoding plasmids, PCR amplification was carried out using ATM_A x D-F and Cel-I-ATM_A-F primers (Table S4 in Supporting Information). Detection of chromosomal translocations was carried out by PCR using Cel-I-ATM_A-F and Cel-I-HPRT1_E-R or Cel-I-HPRT1_E-F and Cel-I-ATM_A-R primers (Table S4 in Supporting Information) for cells transfected with *ATM*_A and *HPRT1*_E TALEN-encoding plasmids. The products were analyzed by electrophoresis in 1% or 3% agarose gels and ethidium bromide staining.

Acknowledgements

We thank Hiroshi Ochiai for providing the HCT116 cells. Part of this work was carried out at the Analysis Center of Life Science, Natural Science Center for Basic Research and Development, Hiroshima University.

References

Brunet, E., Simsek, D., Tomishima, M., DeKelver, R., Choi, V.M., Gregory, P., Urnov, F., Weinstock, D.M. & Jasin, M. (2009) Chromosomal translocations induced at specified loci in human stem cells. *Proc. Natl Acad. Sci. USA* **106**, 10620–10625.

Cermak, T., Doyle, E.L., Christian, M., Wang, L., Zhang, Y., Schmidt, C., Baller, J.A., Somia, N.V., Bogdanove, A.J. & Voytas, D.F. (2011) Efficient design and assembly of custom TALEN and other TAL effector-based constructs for DNA targeting. *Nucleic Acids Res.* **39**, e82.

Ding, Q., Lee, Y.K., Schaefer, E.A., *et al.* (2013) A TALEN genome-editing system for generating human stem cell-based disease models. *Cell Stem Cell* **12**, 238–251.

Doyle, E.L., Booher, N.J., Standage, D.S., Voytas, D.F., Brendel, V.P., Vandyk, J.K. & Bogdanove, A.J. (2012) TAL Effector-Nucleotide Targeter (TALE-NT) 2.0: tools for TAL effector design and target prediction. *Nucleic Acids Res.* **40**, W117–W122.

Gupta, A., Hall, V.L., Kok, F.O., Shin, M., McNulty, J.C., Lawson, N.D. & Wolfe, S.A. (2013) Targeted chromosomal deletions and inversions in zebrafish. *Genome Res.* **23**, 1008–1017.

Hansen, K., Coussens, M.J., Sago, J., Subramanian, S., Gjoka, M. & Briner, D. (2012) Genome editing with CompoZr custom zinc finger nucleases (ZFNs). *J. Vis. Exp.* e3304.

Hockemeyer, D., Wang, H., Kiani, S., *et al.* (2011) Genetic engineering of human pluripotent cells using TALE nucleases. *Nat. Biotechnol.* **29**, 731–734.

Joung, J.K. & Sander, J.D. (2013) TALENs: a widely applicable technology for targeted genome editing. *Nat. Rev. Mol. Cell Biol.* **14**, 49–55.

Kim, H., Kim, M.S., Wee, G., Lee, C.I. & Kim, J.S. (2013a) Magnetic separation and antibiotics selection enable enrichment of cells with ZFN/TALEN-induced mutations. *PLoS ONE* **8**, e56476.

Kim, H., Um, E., Cho, S.R., Jung, C. & Kim, J.S. (2011) Surrogate reporters for enrichment of cells with nuclease-induced mutations. *Nat. Methods* **8**, 941–943.

Kim, Y., Kweon, J., Kim, A., *et al.* (2013b) A library of TAL effector nucleases spanning the human genome. *Nat. Biotechnol.* **31**, 251–258.

Lee, H.J., Kim, E. & Kim, J.S. (2010) Targeted chromosomal deletions in human cells using zinc finger nucleases. *Genome Res.* **20**, 81–89.

Lee, H.J., Kweon, J., Kim, E., Kim, S. & Kim, J.S. (2012) Targeted chromosomal duplications and inversions in the human genome using zinc finger nucleases. *Genome Res.* **22**, 539–548.

© 2014 The Authors
Genes to Cells © 2014 by the Molecular Biology Society of Japan and Wiley Publishing Asia Pty Ltd

Liu, Y., Luo, D., Zhao, H., Zhu, Z., Hu, W. & Cheng, C.H. (2013) Inheritable and precise large genomic deletions of non-coding RNA genes in zebrafish using TALENs. *PLoS ONE* **8**, e76387.

Moehle, E.A., Rock, J.M., Lee, Y.L., Jouvenot, Y., DeKelver, R.C., Dekelver, R.C., Gregory, P.D., Urnov, F.D. & Holmes, M.C. (2007) Targeted gene addition into a specified location in the human genome using designed zinc finger nucleases. *Proc. Natl Acad. Sci. USA* **104**, 3055–3060.

Piganeau, M., Ghezraoui, H., De Cian, A., Guittat, L., Tomishima, M., Perrouault, L., René, O., Katibah, G.E., Zhang, L., Holmes, M.C., Doyon, Y., Concordet, J.P., Giovannangeli, C., Jasin, M. & Brunet, E. (2013) Cancer translocations in human cells induced by zinc finger and TALE nucleases. *Genome Res.* **23**, 1182–1193.

Sakuma, T., Hosoi, S., Woltjen, K., Suzuki, K., Kashiwagi, K., Wada, H., Ochiai, H., Miyamoto, T., Kawai, N., Sasakura, Y., Matsuura, S., Okada, Y., Kawahara, A., Hayashi, S. & Yamamoto, T. (2013) Efficient TALEN construction and evaluation methods for human cell and animal applications. *Genes Cells* **18**, 315–326.

Santiago, Y., Chan, E., Liu, P.Q., Orlando, S., Zhang, L., Urnov, F.D., Holmes, M.C., Guschin, D., Waite, A., Miller, J.C., Rebar, E.J., Gregory, P.D., Klug, A. & Collingwood, T.N. (2008) Targeted gene knockout in mammalian cells by using engineered zinc-finger nucleases. *Proc. Natl Acad. Sci. USA* **105**, 5809–5814.

Urnov, F.D., Rebar, E.J., Holmes, M.C., Zhang, H.S. & Gregory, P.D. (2010) Genome editing with engineered zinc finger nucleases. *Nat. Rev. Genet.* **11**, 636–646.

Xiao, A., Wang, Z., Hu, Y., Wu, Y., Luo, Z., Yang, Z., Zu, Y., Li, W., Huang, P., Tong, X., Zhu, Z., Lin, S. & Zhang, B. (2013) Chromosomal deletions and inversions mediated by TALENs and CRISPR/Cas in zebrafish. *Nucleic Acids Res.* **41**, e141.

Received: 31 October 2013
Accepted: 22 January 2014

Supporting Information

Additional Supporting Information may be found in the online version of this article at the publisher's web site:

Table S1 Primers for construction of TALEN and fluorescent protein co-expression vectors

Table S2 Nucleotide sequences of TALEN target sites

Table S3 Combinations of TALEN arrays and vectors used

Table S4 Primers for amplifying DNA fragments around the target sites

Table S5 Indexes of numbers and percentages of collected cells. Approximately, twice the number of counted cells represented below was collected for the actual genomic analyses

© 2014 The Authors
Genes to Cells © 2014 by the Molecular Biology Society of Japan and Wiley Publishing Asia Pty Ltd

REVIEW

Hepatoblastoma state of the art: pathology, genetics, risk stratification, and chemotherapy

Piotr Czauderna[a], *Dolores Lopez-Terrada*[b], *Eiso Hiyama*[c], *Beate Häberle*[d], *Marcio H. Malogolowkin*[e], *and Rebecka L. Meyers*[f]

Purpose of review
As a rare pediatric tumor, hepatoblastoma presents challenges to the individual practitioner as no center will see more than a handful of cases each year.

Recent findings
The Children's Hepatic tumor International Collaborative (CHIC) effort has fostered international cooperation in this rare children's tumor, leading to the establishment of a large international collaborative dataset, the CHIC database, which has been interrogated to refine risk stratification and inform treatment options. Apace with this effort has been the international collaboration of pediatric pathologists working together to establish a new international histopathologic consensus classification for pediatric liver tumors as a whole, with particular focus on the histological subtypes of hepatoblastoma.

Summary
International collaborative efforts in hepatoblastoma have led to a new international histopathologic consensus classification, refinements in risk stratification, advances in chemotherapy, and a better understanding of surgical resection options forming the foundation for the development of an upcoming international therapeutic trial.

Keywords
chemotherapy, genetics, hepatoblastoma, pathology, risk stratification

INTRODUCTION

This is part one of a two-part state of the art – hepatoblastoma. The companion, part two, article deals with *PRE-T*reatment *EXT*ent of tumor (PRETEXT) radiographic staging, surgical guidelines and liver transplantation and also appears in this issue. Over the last 4 decades, overall survival in hepatoblastoma has increased from roughly 30% to over 80%, primarily because of advances in chemotherapy and in our ability to achieve complete surgical resection, even in the most advanced of tumors. Detailed herein are some of the key advances in histopathology, epidemiology, genetics, chemotherapy, and risk stratification that have helped drive the improved survival seen in hepatoblastoma.

HISTOPATHOLOGY AND EPIDEMIOLOGY OF HEPATOBLASTOMA

Although primary liver tumors are rare in children, hepatoblastoma is the most common primary pediatric liver tumor, usually diagnosed during the first 3 years of life [1]. Most cases of hepatoblastoma are sporadic; however, some are associated with constitutional genetic abnormalities, malformations, and familial cancer syndromes, such as Beckwith–Wiedemann syndrome (BWS) and familial adenomatous polyposis (FAP) [2–4]. Recent pediatric cancer epidemiological studies, including the US National Cancer Institute Surveillance Epidemiology and End Results (SEER), as well as others in Japan and Europe [5,6], report an average

[a]Department of Surgery and Urology for Children and Adolescents, Medical University of Gdansk, Gdansk, Poland, [b]Department of Pathology, Texas Children's Hospital and Baylor College of Medicine, Houston, Texas, USA, [c]Department of Surgery, Natural Science Center for Basic Research and Development, Hiroshima University Hospital, Hiroshima, Japan, [d]Children's Hospital, Ludwig-Maximilians-University, Munich, Germany, [e]Department of Pediatric Hematology and Oncology, Children's Hospital of Wisconsin, Milwaukee, Wisconsin and [f]Department of Pediatric Surgery, Primary Children's Medical Center, University of Utah, Salt Lake City, Utah, USA

Correspondence to Rebecka L. Meyers, MD, Professor of Pediatric Surgery, University of Utah, Pediatric Surgery Suite 2600, Primary Children's Medical Center, 100 Mario Capecchi Drive, Salt Lake City, UT 84103, USA. Tel: +1 801 662 2950; e-mail: rebecka.meyers@imail.org

Curr Opin Pediatr 2014, 26:19–28
DOI:10.1097/MOP.0000000000000046

Copyright © Lippincott Williams & Wilkins. Unauthorized reproduction of this article is prohibited.

KEY POINTS

- New international pediatric hepatoblastoma consensus classification (Table 1) includes histological subtypes and categories, recognizing how challenging some tumors are to classify, particularly after chemotherapy.
- CHIC risk factor analysis (Table 3) shows refined prognostic estimates in smaller subgroups than previously possible by interrogating a collaborative dataset that includes comprehensive data on 1605 children treated by the four major hepatoblastoma study groups between 1989 and 2008.
- SIOPEL 4 shows an impressive improvement in survival for metastatic patients using a novel schema that incorporated weekly dose-dense cisplatin chemotherapy (Table 6).
- COG, SIOPEL/GPOH, and JPLT are now collaborating to develop a cooperative international hepatoblastoma trial, fostering our ability to compare the historic differences between the chemotherapeutic and surgical approaches of different study groups and enhance biologic study in this rare tumor.

annual percentage increase in the incidence of hepatoblastoma during the last 30 years. Indeed, the incidence does seem to be slowly increasing, with a current rate of 1.2–1.5 cases/million population/year. Because premature birth and very low birth weight have been found to be associated with the later appearance of hepatoblastoma, increase in these patient cohorts may be driving the increase in incidence [7▪]. Oxygen therapy, medications such as furosemide, Total Parenteral Nutrition (TPN), radiation, plasticizers, and other toxins are postulated to perhaps play a role, but the exact mechanisms are not yet understood.

Hepatoblastoma is an embryonal tumor thought to originate from a hepatocyte precursor cell (hepatoblast) that often recapitulates the stages of liver development, displaying a combination of histological patterns [8]. Clinical trials have demonstrated that, in addition to staging, some histological types are also associated with prognosis [9]. One early review showed that 67% of hepatoblastomas were epithelial, with a combination of mixed embryonal and fetal patterns, and 21% displayed a mesenchymal component in addition to the common epithelial patterns. Most importantly, approximately 7% of the total were composed of a pure, well differentiated fetal (WDF) epithelial component, and 5% demonstrated primitive appearing or so-called small cell undifferentiated (SCU) tumor cells [10]. Since then, several studies have demonstrated a correlation between improved survival and WDF histology composed only of cells resembling fetal hepatocytes with minimal mitotic activity. In a recent Children's Oncology Group (COG) publication, Malogolowkin *et al.* [11] reported that, whenever complete tumor specimens can be resected and evaluated prior to chemotherapy, patients with WDF histology [formerly referred to as pure fetal histology (PFH)] and low mitotic activity may be treated exclusively with surgery, and no chemotherapy is necessary. Patients with WDF/PFH histology completely resected upfront and receiving no postoperative chemotherapy comprised 7% of the total number of patients (COG studies INT-0098 and P9645) and showed 100% event-free survival (EFS). This is in striking contrast to other international protocols, which historically have treated all children with liver tumors and elevated alphafetoprotein (AFP) with chemotherapy prior to surgical resection [12▪▪]. It is important to remember, though, that most hepatoblastomas are extremely heterogeneous, often with closely intermixed histological components, and only rarely composed of a single histological type [13▪▪].

A second histological subtype worth mentioning is the SCU. This may be part of an otherwise typical hepatoblastoma, representing a component intermixed with other histologies or present as the sole component in the so-called 'pure small cell' hepatoblastoma. This histologic pattern is sometimes associated with low serum AFP levels and poor response to chemotherapy. The first report regarding the negative association of SCU component was by Kasai and Watanabe, followed by Haas's Children's Cancer Group–Pediatric Oncology Group (CCG–POG, also referred to as COG legacy groups) report, in which none of the patients with small cell hepatoblastoma survived 24 months after the diagnosis [14,15]. Trobaugh-Lotrario *et al.* [16] recently reviewed a large series of hepatoblastoma with small cell histology and confirmed 11 patients with SCU hepatoblastomas presenting with clinically normal or minimally increased serum AFP levels, none of whom survived. Interestingly, six of these tumors were *INI1* nuclear negative by immunohistochemical staining and three of them demonstrated cytogenetic and molecular abnormalities similar to those seen in rhabdoid tumors, suggesting that some, but not all, of these tumors may represent *INI1*-negative neoplasms within the spectrum of primary rhabdoid tumors. However, the significance of small cell component when admixed with other epithelial types, and whether these small foci are sometimes *INI1* expressing, is still under investigation. Participants in the Los Angeles 2011 International Pathology Pediatric Liver Symposium agreed upon a panel of immunohistochemical stains

Copyright © Lippincott Williams & Wilkins. Unauthorized reproduction of this article is prohibited.

including *INI1*, which should be closely correlated with the morphology in order to further characterize this pattern and its prognostic significance. In addition, the group recommended that all *INI1*-negative tumors should be submitted for molecular testing, and patients and family members referred to a genetic counselor to possibly be screened for germline mutations whenever appropriate [13▪▪].

The rarity of hepatoblastoma, combined with the rarity of upfront resection, has resulted in a paucity of complete annotated prechemotherapy specimens, compromising biology studies. Therefore, several international conferences have been sponsored to foster international collaboration and clinical trials. As a result of these meetings, recommendations were outlined for submission, sampling, and evaluation of pediatric liver tumor samples, including minimum diagnostic specimen requirements and evaluation of the uninvolved liver, as well as the necessity of providing minimal clinical information to the reviewer, which should always include age, AFP level at the time of diagnosis, underlying liver disease, and correlation with imaging [13▪▪]. There was also consensus between the pathologists regarding the importance of obtaining prechemotherapy specimens for the initial diagnoses and tumor classification. Finally, the group also highlighted the importance of tissue banking for biological studies [13▪▪].

The newly proposed pathology consensus of pediatric hepatoblastoma classification (Table 1) [13▪▪] includes all prognostically relevant histological types (WDF and SCU), as well as the new categories ('pleomorphic epithelial' and 'malignant hepatocellular neoplasm'), recognizing how challenging some tumors are to classify, particularly after chemotherapy. Reviewers also highlighted the importance of appropriately sampling and following specimen submission recommendations, as well as the imperative need to characterize the biology of hepatoblastoma, pediatric hepatocellular carcinoma, and other hepatocellular neoplasms, and to identify biological markers that could be used for tumor classification, clinical stratification, and to develop new novel therapeutic strategies.

Table 1. International consensus classification of the histologic subtypes of hepatoblastoma

Epithelial	Subtype/definition	Mixed	Subtype/definition
Fetal	Well differentiated and uniform (10–20 μm diameter), round nuclei, cords with minimal mitotic activity, EMH	Stromal derivatives	Spindle cells (blastema), osteoid, skeletal muscle, cartilage
	Crowded or mitotically active (>2 per 10 400× microscopic fields); conspicuous nucleoli (usually less glycogen)	Teratoid	Mixed, plus primitive endoderm; neural derivatives, melanin, squamous and glandular elements
	Pleomorphic, poorly differentiated Moderate anisonucleosis, high N/C, nucleoli		
	Anaplastic with marked nuclear enlargement and pleomorphism, hyperchromasia, abnormal mitoses		
Embryonal	10–15 μm diameter, high N/C, angular, primitive tubules, EMH		
Macrotrabecular	Epithelial HB (fetal or embryonal) growing in clusters of >5 cells between sinusoids		
Small cell undifferentiated (SCU)	(5–10 μm diameter) no architectural pattern, minimal pale amphophilic cytoplasm, round to oval nuclei with fine chromatin and inconspicuous nucleoli, +/- mitoses; +/- INI[a]		
Cholangioblastic	Bile ducts, usually at periphery of epithelial islands, can predominate		

EMH, extramedullary hematopoiesis; HB, hepatoblastoma. Data from [13▪▪]

[a]Pure small cell undifferentiated needs to be differentiated from malignant rhabdoid tumors (discohesive, eccentric irregular nuclei, prominent nucleoli, abundant cytoplasmic filaments including cytokeratin and vimentin, negative nuclear INI).

Copyright © Lippincott Williams & Wilkins. Unauthorized reproduction of this article is prohibited.

PREDICTING PROGNOSIS: GENETICS

Several prognostic markers and constitutional genetic syndromes such as Trisomy 18/Edward's syndrome, BWS, and FAP have been reported in association with hepatoblastoma [17]. There have been at least seven published cases of hepatoblastoma in children with trisomy 18/Edward's syndrome. BWS predisposes to a number of embryonal tumors and the overall percentage of children with BWS who develop tumors is 7.5–13.5%, with the most frequent tumors being Wilms' tumor and hepatoblastoma. Regarding FAP, it appears that there may be genotype–phenotype links between specific mutations to the *APC* gene, which is mutated in FAP. In families with FAP and hepatoblastoma, referral to a genetic counselor is recommended.

The most frequent genetic aberrations (70–90%) in hepatoblastoma occur in genes involved in the *Wnt* signaling pathway [18,19]. A majority of hepatoblastoma have *Wnt* signal abnormalities. Recently, telomerase activation and genetic expression profiles were identified as prognostic factors [20,21]. Among 212 hepatoblastoma enrolled in Japanese Study Group for Pediatric Liver Tumors (JPLT)-2 between 2000 and 2010, large deletion of *CTNNB1* was detected in 107 cases and mutation of *CTNNB1* exon 3 was detected in 56 cases. Approximately 80% had abnormalities of these factors, including *APC* and *Axin* genes. Immunohistochemistry revealed β-catenin was accumulated in the tumor cells with *Wnt* signal aberrations. Not all, but a majority, of the samples showed elevated expression of *Wnt* signal target genes such as *cyclin D1*, *survivin*, and *MYC*.

Telomerase, the activated enzyme related to cell immortality, is a reverse transcriptase for the elongation of telomeres, is regulated by the expression of *TERT* (human telomerase reverse transcriptase), and is a catalytic component of human telomerase [22,23]. *Wnt* signal activation usually occurs in aggressive tumors, *TERT* expression plays a major role in *Wnt* signal activation, and *MYC* (an activated *Wnt* signal target gene) enhances *TERT* expression. As a result, activation of *TERT* and *MYC* signaling appears to play a role in the more aggressive phenotypes of hepatoblastoma [24,25]. Additionally, recent microarray analysis by Cairo and colleagues revealed a 16-gene signature that discriminated invasive and metastatic hepatoblastoma and predicted prognosis. These 16 genes were the highly proliferating subclass typified by upregulated *MYC* signaling [26]. These findings support the *MYC* activation theory by *Wnt* signaling activation in aggressive hepatoblastoma, again suggesting that a *TERT* and *MYC* vicious cycle may exist in aggressive tumors.

PREDICTING PROGNOSIS: RISK STRATIFICATION AND CLINICAL PROGNOSTIC FACTORS

The four major study groups – International childhood liver tumors strategy group (SIOPEL), COG, German Society for Pediatric Oncology (GPOH), and JPLT – have historically had disparate risk classification categories, making it difficult to compare the outcomes across the oceans. Fortunately, all groups have increasingly used the PRETEXT grouping system for risk stratification, as discussed in Part Two of this review. Over the last 10 years, individual study groups have attempted to define the relative importance of a variety of suspected prognostic factors present at diagnosis and in response to therapy [9,11,27,28,29▪▪,30] (Table 2). In SIOPEL, good prognostic factors have included low PRETEXT at diagnosis (PRETEXT I, II, and III tumors) [28]. In COG, good prognosis has been shown for Stage I tumors resected at diagnosis and tumors with pure fetal histology [9,11]. Poor prognostic factors identified individually in these trials include PRETEXT IV, metastatic disease, AFP less than 100, and SCU histology [9,27]. Other variables such as tumor rupture prior to diagnosis, tumor multifocality, macrovascular tumor invasion, extrahepatic tumor extension, age at diagnosis, very high (>1.2 million) or borderline low (100–1000) AFP have been

Table 2. Potential prognostic factors in hepatoblastoma

Pre-treatment	Response to treatment
PRETEXT (I[a], II[a], III, IV[d])	Response to chemotherapy
Metastasis at diagnosis[b]	Positive surgical margins
Unresectable vessel involvement (+V, +P)[b]	Surgical resectability
Extrahepatic tumor extension (+E)[b]	Tumor relapse
Lymph nodes	
Multifocal tumor[b]	
Tumor rupture at diagnosis[b]	
AFP level (<100[b]; 100–1000[b]; >1 million)	
Pathologic subtype (pure fetal[c], small cell undifferentiated[d])	
Age (<1 year[a]; >6 years[b])	
Birth weight	
Platelet count	
Co-morbidity	

AFP, alphafetoprotein; CHIC, Children's Hepatic tumor International Collaboration.
[a]Good prognostic factor in CHIC multivariate analysis [30].
[b]Poor prognostic factor in CHIC multivariate analysis [30].
[c]Good prognostic factor [11].
[d]Poor prognostic factor [9,28,29▪▪].

Copyright © Lippincott Williams & Wilkins. Unauthorized reproduction of this article is prohibited.

suggested as poor prognostic factors, but the relative importance of their prognostic significance has been difficult to define [29▪▪]. Factors in response to treatment that had been hypothesized as poor prognostic factors include poor response or progressive disease on chemotherapy, gross positive surgical margins, surgically unresectable tumor, and tumor relapse.

Efforts to define clinical prognosis in hepatoblastoma have historically been challenging because of the low numbers of patients, even in multicenter trials. To address this challenge, the Children's Hepatic tumor International Collaboration (CHIC) initiative was formed to combine the results of multicenter trials by SIOPEL, COG, JPLT, and GPOH over the last 20 years and thereby gain enhanced statistical power with increased numbers. In cooperation with the data management group Consorzio Interuniversitario (CINECA), CHIC created a dataset that includes comprehensive data on all children treated in 11 separate trials by the four major hepatoblastoma study groups between 1989 and 2008, a total of 1605 patients [31]. Univariate analysis was used to identify statistically significant prognostic variables, which were then included in a backwards elimination multivariate analysis to identify those constellations of variables most predictive of outcome [30]. Factors significant by univariate analysis at diagnosis were PRETEXT, AFP less than 100, AFP 100–1000, metastatic disease, age group, macrovascular involvement vena cava/hepatic veins (+V), macrovascular involvement portal veins (+P), contiguous extrahepatic tumor (E), multifocal disease, and spontaneous rupture at diagnosis. Multivariate analysis of these factors led to the selection of a risk backbone based upon PRETEXT I/II, PRETEXT III, PRETEXT IV, AFP less than 100, and metastatic disease. Within each of these backbone groups, the presence or absence of the remaining risk factors was further stratified by multivariate estimates of EFS (Table 3) [30]. This statistical effort is ongoing and has not yet been rigorously validated. Upon maturation of outcome data from the current COG trial, AHEP0731, the CHIC group hopes to combine the data of AHEP0731 and SIOPEL 4 to form a validation set for the CHIC risk groups. Moreover, validation and refinement of these risk groups is one of the primary objectives in the planning for an upcoming international collaborative hepatoblastoma therapeutic trial.

HEPATOBLASTOMA MULTICENTER TRIALS

Treatment of hepatoblastoma in children represents a true success story of pediatric oncology in the last 25 years. From prechemotherapy survival rates in

Table 3. Multivariate analysis of risk groups in the Children's Hepatic tumor International Collaboration (CHIC) database

PRETEXT	Age (years)	AFP	Other risk factors[a] (0, 1, ≥2)	# Patients in CHIC database[b]	5-Year EFS
I and II	<3	>100	0	375	92%
III	<1	>1000	0	125	91%
I and II	<3	>100	≥1	50	76%
I and II	3–5	>100	Any	53	74%
III	<1	>1000	≥1	43	83–86%
III	>1	>1000	0	134	87%
III	>1	>1000	1	42	74%
IV	<3	>100	0	58	77%
I and II	>6	>100	Any	28	51%
III	Any	100–1000	Any	28	61%
IV	<3	>100	1	59	66%
III	>1	>1000	>1	24	50%
IV	<3	>100	>1	32	46%
IV	>3	>100	Any	40	31%
M+ (any pretext)	Any	>100	Any and Pretext 4	259	18–48%
AFP <100 (any pretext)	Any	–	Any	65	36%

AFP, alphafetoprotein. Data from [30].
[a]Other risk factors statistically significant in multivariate analysis: multifocal tumor, major venous involvement +V (all three hepatic veins or inferior vena cava), major venous involvement +P (portal bifurcation or both portal veins), extrahepatic contiguous tumor extension +E, and tumor rupture.
[b]CHIC database includes patients from COG (INT-0098; P9645); SIOPEL (SIOPEL-2; SIOPEL-3SR, SIOPEL-3HR); JPLT (JPLT-1; JPLT-2); and GPOH (HB89; HB 99).

Copyright © Lippincott Williams & Wilkins. Unauthorized reproduction of this article is prohibited.

the 1970s of 30%, the use of adjuvant and neoadjuvant chemotherapy brought the patients' survival to 70–80%. This progress was possible not only because of the introduction of new drugs (i.e. cisplatin and doxorubicin), but also because of the new surgical approaches (i.e. hepatic exclusion, Pringle, ultrasonic dissection, liver transplantation) and, perhaps most importantly, because of multicenter cooperative efforts of the major international study groups (Table 4) [27,32–39].

One fundamental controversy between various study groups has been the issue of primary hepatic resection, with SIOPEL recommending preoperative chemotherapy in every case, in every patient, and in every tumor. The other groups have traditionally carved out some lower-risk groups amenable to upfront resection. The initial American approach (INT-0098,P9645) put the upfront surgical decision in the hands of the individual surgeon and recommended an attempt at upfront resection in everyone. The old COG Evan's stages I, II, and III were based upon the surgeon's success or failure to resect the tumor at diagnosis. In those who were not 'resectable', biopsy only was performed, followed by chemotherapy, delayed surgery, and postoperative chemotherapy. In those who were resectable, a primary partial hepatectomy was followed by postoperative chemotherapy [39]. The current COG trial, AHEP-0731, has moved away from putting surgical decisions arbitrarily in the hands of an individual surgeon. This study's surgical guidelines recommend upfront resection only for PRETEXT I and II tumors, when the diagnostic imaging shows clear radiographic margins on the contralateral portal vein, the middle hepatic vein, and the retrohepatic inferior vena cava [40].

The evolution of chemotherapeutic approaches is well illustrated by following the progression of results shown in Table 4. Contemporary chemotherapy protocols from the four major study groups

Table 4. Summary results of hepatoblastoma cooperative trials

Study	Chemotherapy	Number of patients	Outcomes
INT0098 (CCG/POG) 1989–1992	C5V vs. CDDP/DOXO	Stage: I/II: 50; Stage III: 83; Stage IV: 40	4-Year EFS/OS: I/II = 88%/100% vs. 96%/96%; III = 60%/68% vs. 68%/71%; IV = 14%/33% vs. 37%/42%
P9645 (COG) 1999–2002	C5V vs. CDDP/CARBO	Stage: I/II: pending publication; Stage III = 38; Stage IV = 50	1-Year EFS[a]: Stage III/IV: C5V 51%; CDDP/Carbo 37%
HB 94 (GPOH) 1994–1997	I/II: IFOS/CDDP/DOXO; III/IV: IFOS/CDDP/ DOXO + VP/CARBO	Stage: I: 27; II: 3; III: 25; IV: 14	4-Year EFS/OS: I = 89%/96%; II = 100%/100%; III = 68%/76%; IV = 21%/36%
HB 99 (GPOH) 1999–2004	SR: IPA; HR: CARBO/VP16	SR: 58; HR: 42	3-Year EFS/OS: SR: 90%/88%; HR: 52%/55%
SIOPEL 2 1994–1998	SR: PLADO; HR: CDDP/ CARBO/DOXO	PRETEXT: I = 6; II = 36; III = 25; IV = 21; Mets: 25	3-Year EFS/OS: SR: 73%/91%; HR: IV = 48%/61%; HR: Mets: 36%/44%
SIOPEL 3 1998–2006	SR: CDDP vs. PLADO; HR: SUPERPLADO	SR: PRETEXT I = 18; II = 133; III = 104; HR: PRETEXT IV = 74; +VPE = 70; Mets = 70; AFP <100 = 12	3-Year EFS/OS: SR: CDDP 83%/95%; PLADO 85%/93%; HR: overall 65%/69%; Mets 57%/63%
SIOPEL 4 2005–2009	HR: Block A: Weekly; CDDP/3 weekly DOXO; Block B CARBO/DOXO	PRETEXT: I = 2; II = 17; III = 27; IV = 16; Mets= 39	3-Year EFS/OS: All HR = 76%/83%; HR: IV = 75%/88%; HR: Mets: 77%/79%
JPLT 1 1991–1999	I/II: CDDP(30)/THPA-DOXO; III/IV: CDDP(60)/THPA-DOXO	Stage: I: 9; II: 32; IIIa: 48; IIIb: 25; IV: 20	5-Year EFS/OS: I = ? /100%; II = ?/76%; IIa = ?/50%; IIIb = ?/64%; IV = ?/77%
JPLT 2 1999–2010	I: low-dose CDDP Pirarubicin; II–IV: CITA Mets: High dose + stem cell transplant	Stage: n = 212; PRETEXT I: 95; II: 95; III: 100; IV: 48; Mets: 46	5-Year EFS/OS: I = ?/100%; II = ?/89%; III = ?/93%; IV = ?/63%; Mets 32%

AFP, alphafetoprotein; CARBO, carboplatin; CCG, Children's Cancer Group; CDDP, cisplatin; CITA, Cisplatin/Pirarubicin; COG, Children's Oncology Group; C5V, cisplatin + 5-fluorouracil (5FU) + vincristine; DOXO, doxorubicin; EFS, event-free survival; GPOH, German Society for Pediatric Oncology; HR, high risk; IFOS, ifosfamide; JPLT, Japanese Study Group for Pediatric Liver Tumors; Mets, metastatic; OS, overall survival; PLADO, cisplatin + doxorubicin; POG, Pediatric Oncology Group; PRETEXT, pre-treatment extent of tumor; SIOPEL, international childhood liver tumors strategy group; SR, standard risk; SUPERPLADO, cisplatin+ doxorubicin + carboplatin; THPA, tetrahydropyranyl adriamycin; VP, etoposide. Data from [27,32–38].
[a]Study closed early because of inferior results in CDDP/CARBO arm.

Copyright © Lippincott Williams & Wilkins. Unauthorized reproduction of this article is prohibited.

Table 5. Current chemotherapy recommendations of the different study groups

Study group	Risk group	Chemotherapy	Surgery
COG (AHEP 0731)	Very low risk	None	Primary
	Low risk	CDDP, 5FU, VCR × 2	Primary
	Intermediate risk	CDDP, 5FU, VCR, Doxo × 6–8	After 2–4 courses
	High risk	VCR, irinotecan, temsirolimus × 2	After 4–6 courses
		CDDP, 5FU, VCR, Doxo × 6	
SIOPEL (SIOPEL 6)	Standard risk	CDDP × 6	After 4 courses
(SIOPEL 4)	High risk	CDDP weekly × 8, Doxo 3rd weekly × 3	After 8 CDDP/3 Doxo
GPOH	Standard risk	CDDP, Doxo × 3–4	After 2–3 courses
	High risk	CDDP × 5 alternating CARBO/ Doxo × 5 (SIOPEL 3 HR)	After 5–7 courses
JPLT (JPLT 2)	PRETEXT I	CDDP, PIRA × 4	Primary
	PRETEXT II	CDDP, PIRA × 6	After 2 courses
	PRETEXT III/IV all V+P+E+	CDDP, PIRA × 5–6 or CDDP, PIRA × 2 + IFOS/CARBO/ PIRA/ETO × 3–4	After 3–4 courses
	All PRETEXT M+	Additional high-dose ETO/CARBO/MEL	After 4 courses

5-FU, 5-fluorouracil; CARBO, carboplatin; CDDP, cisplatin; COG, Children's Oncology Group; Doxo, doxorubicin; ETO, etoposide; GPOH, German Society for Pediatric Oncology; HR, high risk; IFOS, ifosfamide; JPLT, Japanese Study Group for Pediatric Liver Tumors; MEL, Melphalan; PIRA, pirarubicin; PRETEXT, pre-treatment extent of tumor; VCR, vincristine. Data from [12▪▪,33,38,41▪▪,42].

are shown in Table 5 [12▪▪,33,38,41▪▪,42]. The SIOPEL 1, 2, 3, 4 series of studies have shown progressive improvements in survival, especially in the high-risk (hepatoblastoma – high risk) cohorts (Table 6) [34–36,41▪▪,42]. SIOPEL 4 shows an impressive improvement in survival for metastatic patients using a novel schema that incorporated weekly dose-dense cisplatin chemotherapy. The results are startling and strike one as almost too good to be true, with 98% (60 of 61 evaluable patients) experiencing a partial response and only 1 of 20 who achieved a pulmonary complete response having relapse [43]. As a single-arm trial, SIOPEL 4 was not randomized; rather, outcomes were compared with historical controls, and therefore further study will be needed before it can be adopted as the standard of care. A total of 97% of patients had grade 3–4 hematologic toxicity. This is consistent with some adult studies that have used a similar approach and may be considered acceptable. However, fever and neutropenia occurred in 71% of patients and four patients had toxic deaths (two from infection, one from surgical bleeding, and one with tumor bleeding). The number of patients with significant hearing loss was greater than 50%. As ototoxicity is difficult to measure, notoriously underreported, and can progress over time, the question remains as to what hearing function these very young patients will have in the long run. The SIOPEL 4 results suggest that this regimen should be compared in a randomized trial, further evaluating the toxicities of this design, and, in fact, planning is underway to study this regimen in the high-risk arm of a new international trial being planned as a joint effort between COG, SIOPEL/GPOH, and JPLT. Additionally, as exciting as these results are, it

Table 6. Progression of high-risk outcomes in SIOPEL studies over the last 2 decades

	SIOPEL 1 High risk	SIOPEL 2 High risk	SIOPEL 3 High risk	SIOPEL 4 High risk
Response rate	78%	76%	77.5%	97%
Complete resection rate	58%	66%	69%	87%
EFS 3 years	45%	47%	65%	80%*
OS 3 years	57%	52%	73%	82%*
EFS metastatic	28%	44%	56%	80%*
EFS Pretext 4	46%	61%	68%	81%*

EFS, event-free survival; OS, overall survival; Pretext, pre-treatment extent of tumor; SIOPEL, international childhood liver tumors strategy group. Data from [34–36,41▪▪,42].

Copyright © Lippincott Williams & Wilkins. Unauthorized reproduction of this article is prohibited.

emphasizes the urgent need for new agents to address that subset of tumors that remain unresponsive.

Novel strategies have been investigated by JPLT and COG. In JPLT-2, the use of high-dose chemotherapy with autologous stem cell/bone marrow transplant rescue was used in the highest-risk patients, but was not found to improve survival [39]. COG AHEP-0731, in collaboration with JPLT, is studying patients using vincristine–irinotecan and vincristine–irinotecan–temsirolimus in metastatic patients in a novel upfront window design prior to beginning standard COG C5V-D chemotherapy (cisplatin, 5FU, vincristine, and doxorubicin) [44▪].

CHEMOTHERAPY, PROGRESSIVE DISEASE AND TUMOR RELAPSE: NEW DEVELOPMENTS IN CHEMOTHERAPY

Few conventional chemotherapy agents have demonstrated activity in progressive or relapse hepatoblastoma [45]. Doxorubicin, carboplatin, etoposide, and ifosfamide have been used as part of rescue strategies and have been incorporated in upfront therapy for high-risk patients as well [46–48]. Approximately one-third of the patients whose disease progressed or recurred after initial treatment without anthracyclines could be successfully rescued with a doxorubicin-containing regimen and surgery [46]. Irinotecan has been used experimentally as a maintenance therapy in a handful of patients suspected of being at high risk for relapse [47]. A SIOPEL phase 2 study investigated irinotecan in 28 patients with relapse and progressive disease on conventional chemotherapy. Of the 23 evaluable patients, 6 had a partial response, 11 had stable disease, and 6 had progressive disease. Irinotecan appeared to have significant antitumor activity in a small but real subset of these patients [49]. High-dose chemotherapy with stem cell rescue has been used in the setting of progressive or relapsed hepatoblastoma. However, as the available data is based on case reports or small series with potential for selection bias, the role and efficacy of this approach are still unknown [38,50–52]. Hepatic intra-arterial chemoembolization has been shown to be efficacious in shrinking these tumors and allowing complete surgical resection after initial systemic chemotherapy [53,54]. Surgical resection of relapse nodules in the lungs can be curative, but has a high failure rate [55].

Agents like irinotecan and oxaliplatin have been tested in small numbers of patients with relapse [48,56,57]. Whereas irinotecan has shown to have some activity, no objective response was seen for hepatoblastoma in a phase II study of oxaliplatin [57]. Newer targeted agents that 'selectively' interfere with the pathway targets involved in tumor growth, progression, and vascular development, such as insulin-like growth factor (IGF), phosphatidylinositol 3-kinase (PI3K), mammalian target of rapamycin (mTOR), and vascular endothelial growth factor (VEGF), are currently under development. Gene-directed treatment approaches and immunotherapy have high potential as future treatment options. Both therapy options have displayed promising results in preclinical models so far, but are clearly only in the infancy of their scientific evaluation [58–65].

CONCLUSION

Further understanding of the histopathologic subtypes and molecular mechanisms responsible for the development and progression of these tumors is essential to prioritize the most promising agents for clinical evaluation. International cooperation is necessary for the continuous improvement in the outcomes of these patients and the advancement in the knowledge of the genetics, epidemiology, and biology of these tumors. With the foundation provided by the CHIC, work is now well underway in the formation of a new cooperative international hepatoblastoma trial, fostering our ability to compare the historic differences between the chemotherapeutic and surgical approaches of different study groups and define the true state of the art.

Acknowledgements

Funding for the Children's Hepatic tumor International Collaboration (CHIC) has been provided by grants from European Network for Cancer research in Children and Adolescents (ENCCA),FP-7,#261474; Hepatoblastoma Foundation administered through CureSearch; and Japanese Children's Cancer Foundation.

Conflicts of interest

There are no conflicts of interest.

REFERENCES AND RECOMMENDED READING

Papers of particular interest, published within the annual period of review, have been highlighted as:
- ▪ of special interest
- ▪▪ of outstanding interest

1. López-Terrada D, Finegold MJ. Tumors of the liver. In: Suchy FJ, editor. Liver disease in children. New York: Cambridge University Press; 2012.
2. Garber JE, Li FP, Kingson JE, *et al.* Hepatoblastoma and familial adenomatous polyposis. J Natl Cancer Inst 1988; 80:1626–1628.
3. Cohen MM Jr. Beckwith–Wiedemann syndrome: historical, clinicopathological, and etiopathogenetic perspectives. Pediatr Dev Pathol 2005; 8:287–304.

Copyright © Lippincott Williams & Wilkins. Unauthorized reproduction of this article is prohibited.

4. Thomas D, Pritchard J, Davidson R, *et al.* Familial hepatoblastoma and APC gene mutations: renewed call for molecular research. Eur J Cancer 2003; 39:2200–2204.
5. Buckley JD, Sather H, Ruccione K, *et al.* A case–control study of risk factors for hepatoblastoma. A report from the Childrens Cancer Study Group. Cancer 1989; 64:1169–1176.
6. http://seer.cancer.gov. Surveillance epidemiology and end results website. 2009.
7. Spector LG, Birch J. The epidemiology of hepatoblastoma. Pediatr Blood ▪ Cancer 2012; 59:776–779.

A comprehensive review of hepatoblastoma epidemiology.

8. Finegold MJ, Lopez-Terrada DH, Bowen J, *et al.* Protocol for the examination of specimens from pediatric patients with hepatoblastoma. Arch Pathol Lab Med 2007; 131:520–529.
9. Meyers RL, Rowland JH, Krailo M, *et al.* Pretreatment prognostic factors in hepatoblastoma: a report of the Children's Oncology Group. Pediatr Blood Cancer 2009; 53:1016–1022.
10. Weinberg AG, Finegold MJ. Primary hepatic tumors of childhood. Hum Pathol 1983; 14:512–537.
11. Malogolowkin MH, Katzenstein HM, Meyers RL, *et al.* Complete surgical resection is curative for children with hepatoblastoma with pure fetal histology: a report from the Children's Oncology Group. J Clin Oncol 2011; 29:3301–3306.
12. Perilongo G, Malogolowkin MH, Feusner J. Hepatoblastoma clinical research: ▪▪ lessons learned and future challenges. Pediatr Blood Cancer 2012; 59:818–821.

A comprehensive review of hepatoblastoma chemotherapy.

13. López-Terrada D, Alaggio R, De Dávila MT, *et al.* Towards an International ▪▪ Pediatric Liver Tumor Consensus Classification: Proceedings of the Los Angeles COG International Pathology Pediatric Liver Tumors Symposium. Mod Pathol 2013. [Epub ahead of print].

New hepatoblastoma pathology consensus classification.

14. Kasai M, Watanabe I. Histologic classification of liver-cell carcinoma in infancy and childhood and its clinical evaluation. A study of 70 cases collected in Japan. Cancer 1970; 25:551–563.
15. Haas JE, Feusner J, Finegold MJ. Small cell undifferentiated histology in hepatoblastoma may be unfavorable. Cancer 2001; 92:3130–3134.
16. Trobaugh-Lotrario AD, Tomlinson GE, Finegold MJ, *et al.* Small cell undifferentiated variant of hepatoblastoma: adverse clinical and molecular features similar to rhabdoid tumors. Pediatr Blood Cancer 2009; 52:328–334.
17. Stocker JT. Hepatoblastoma. Semin Diagn Pathol 1994; 11:136–143.
18. Takayasu H, Horie H, Hiyama E, *et al.* Frequent deletions and mutations of the beta-catenin gene are associated with overexpression of cyclin D1 and fibronectin and poorly differentiated histology in childhood hepatoblastoma. Clin Cancer Res 2001; 7:901–908.
19. Anna CH, Sills RC, Foley JF, *et al.* Beta-catenin mutations and protein accumulation in all hepatoblastomas examined from B6C3F1 mice treated with anthraquinone or oxazepam. Cancer Res 2000; 60:2864–2868.
20. Hiyama E, Yamaoka H, Matsunaga T, *et al.* High expression of telomerase is an independent prognostic indicator of poor outcome in hepatoblastoma. Br J Cancer 2004; 91:972–979.
21. Cairo S, Armengol C, De Reynie A, *et al.* Hepatic stem-like phenotype and interplay of Wnt/beta-catenin and Myc signaling in aggressive childhood liver cancer. Cancer Cell 2008; 14:471–484.
22. Hiyama E, Hiyama K, Shay JW, Yokoyama T. Immunohistochemical detection of telomerase (hTERT) protein in human cancer tissues and a subset of cells in normal tissues. Neoplasia 2001; 3:17–26.
23. Hiyama E, Hiyama K. Clinical utility of telomerase in cancer. Oncogene 2002; 21:643–649.
24. Park JI, Venteicher AS, Hong JY, *et al.* Telomerase modulates Wnt signalling by association with target gene chromatin. Nature 2009; 460:66–72.
25. Ueda Y, Hiyama E, Kamimatsuse A, *et al.* Wnt signaling and telomerase activation of hepatoblastoma: correlation with chemosensitivity and surgical resectability. J Pediatr Surg 2011; 46:2221–2227.
26. Armengol C, Cairo S, Fabre M, Buendia MA. Wnt signaling and hepatocarcinogenesis: the hepatoblastoma model. Int J Biochem Cell Biol 2011; 43:265–270.
27. Fuchs J, Rydzynski J, von Schweinitz D, *et al.* Pretreatment prognostic factors and treatment results in children with hepatoblastoma: a report from the German Cooperative Pediatric Liver Tumor Study HB94. Cancer 2002; 95:172–182.
28. Aronson DC, Schnater JM, Staalman CR, *et al.* Predictive value of the pretreatment extent of disease system in hepatoblastoma: results from the international society of pediatric oncology liver tumor study group SIOPEL-1 study. J Clin Oncol 2005; 23:1245–1252.
29. Maibach R, Roebuck D, Brugieres L, *et al.* Prognostic stratification for children ▪▪ with hepatoblastoma: the SIOPEL experience. Eur J Cancer 2012; 48:1543–1549.

A comprehensive risk factor analysis in the SIOPEL database.

30. Meyers RL, Haeberle B, Hiyama E, *et al.* Children's Hepatic Tumor International Collaboration (CHIC): new hepatoblastoma international risk groups. Hong Kong: Abstract SIOP; 2013.
31. Czauderna P, Haeberle B, Hiyama E, *et al.* Children's Hepatic tumors International Collaboration (CHIC) as a model of international global cooperation and clinical research in pediatric rare tumors. Abstract SIOP: London; 2012.
32. Malogolowkin MH, Katzenstein HM, Krailo M, *et al.* Intensified platinum therapy is an ineffective strategy for improving outcome in pediatric patients with advanced hepatoblastoma. J Clin Oncol 2006; 24:2879–2884.
33. Haeberle B, von Schweinitz D. Treatment of hepatoblastoma in German cooperative pediatric liver tumor studies. Front Biosci 2012; 1:493–498.
34. Perilongo G, Shafford E, Maibach R, *et al.* Risk adapted treatment for childhood hepatoblastoma: final report of the second study of the internal society of pediatric oncology, SIOPEL 2. Eur J Cancer 2004; 40:411–421.
35. Perilongo G, Maibach R, Shafford E, *et al.* Cisplatin versus cisplatin plus doxorubicin for standard risk hepatoblastoma. N Engl J Med 2009; 361:1662–1670.
36. Zsiros J, Maibach R, Shafford E, *et al.* Successful treatment of childhood high-risk hepatoblastoma with dose-intensive multiagent chemotherapy and surgery: final results of the SIOPEL-3HR study. J Clin Oncol 2010; 28:2584–2590.
37. Sasaki F, Matsunaga T, Iwafuchi M, *et al.* Outcome of hepatoblastoma treatment with JPLT-1 Protocol-1: a report from the Japanese study group for pediatric liver tumor. J Pediatr Surg 2002; 37:851–856.
38. Hishiki T, Matsunaga T, Sasaki F, Yano M, *et al.* Outcome of hepatoblastoma treated using the Japanese Study Group for Pediatric Liver Tumor (JPLT) protocol-2: report from the JPLT. Pediatr Surg Int 2011; 27:1–8.
39. Ortega JA, Douglass EC, Feusner JH, *et al.* Randomized comparison of cisplatin/vincristin/5-fluorouracil and cisplatin/doxorubicin for the treatment of pediatric hepatoblastoma (HB): A report from the Children's Cancer Group and the Pediatric Oncology Group. J Clin Oncol 2000; 18:2665–2675.
40. Meyers RL, Czauderna P, Otte JB. Surgical treatment of hepatoblastoma. Pediatr Blood Cancer 2012; 59:800–808.
41. Zsiros J, Brugieres L, Brock P, *et al.* Dose-dense cisplatin-based chemother- ▪▪ apy and surgery for children with high risk hepatoblastoma (SIOPEL 4): a prospective, single-arm, feasibility study. Lancet Oncol 2013; 14:834–842.

A recent study with best ever result achieved in metastatic hepatoblastoma.

42. Pritchard J, Brown J, Shafford E, *et al.* Cisplatin, doxorubicin, and delayed surgery for childhood hepatoblastoma: a successful approach – results of the first prospective study of the International Society of Pediatric Oncology. J Clin Oncol 2000; 18:3819–3828.
43. Qayed M, Katzenstein HM. Dose-intensive cisplatin for hepatoblastoma: have you heard? Lancet Oncol 2013; 14:791–792.
44. Troubaugh-Lotrario AD, Katzenstein HM. Chemotherapeutic approaches for ▪ newly diagnosed hepatoblastoma: past, present, and future strategies. Pediatr Blood Cancer 2012; 59:809–812.

A comprehensive review of COG studies.

45. Semeraro M, Branchereau S, Maibach R, *et al.* Relapses in hepatoblastoma patients: clinical characteristics and outcome – experience of the International Childhood Liver Tumour Strategy Group (SIOPEL). Eur J Cancer 2013; 49:915–922.
46. Malogolowkin MH, Katzenstein HM, Krailo M, *et al.* Redefining the role of doxorubicin for the treatment of children with hepatoblastoma. J Clin Oncol 2008; 26:2379–2383.
47. Katzenstein HM, London WB, Douglass EC, *et al.* Treatment of unresectable and metastatic hepatoblastoma: a Pediatric Oncology Group phase II study. J Clin Oncol 2002; 20:3438–3444.
48. Qayed M, Powell C, Morgan ER, *et al.* Irinotecan as maintenance therapy in high-risk hepatoblastoma. Pediatr Blood Cancer 2010; 54:761–763.
49. Zsiros J, Brugieres L, Brock P, *et al.* Efficacy of irinotecan single drug treatment in children with refractory or recurrent hepatoblastoma – a phase II trial of the childhood liver tumour strategy group (SIOPEL). Eur J Cancer 2012; 48:3456–3464.
50. Yoshinari M, Imaizumi M, Hayashi Y, *et al.* Peripheral blood stem cell transplantation for hepatoblastoma with microscopical residue: a therapeutic approach for incompletely resected tumor. Tohoku J Exp Med 1998; 184:247–254.
51. Perilongo G, Otte JB. Autologous peripheral blood stem-cell transplantation with a double-conditioning regimen for recurrent hepatoblastoma after liver transplantation: a valid therapeutic option or just too much? Pediatr Transplant 2009; 13:148–149.
52. Niwa A, Umeda K, Awaya T, *et al.* Successful autologous peripheral blood stem cell transplantation with a double-conditioning regimen for recurrent hepatoblastoma after liver transplantation. Pediatr Transplant 2009; 13:259–262.
53. Malogolowkin MH, Stanley P, Steele DA, *et al.* Feasibility and toxicity of chemoembolization for children with liver tumors. J Clin Oncol 2000; 18:1279–1284.
54. Czauderna P, Zbrzeniak G, Narozanski W, *et al.* Preliminary experience with arterial chemoembolization for hepatoblastoma and hepatocellular carcinoma in children. Pediatr Blood Cancer 2006; 46:825–828.
55. Meyers RL, Katzenstein HM, Krailo M, *et al.* Surgical resection of pulmonary metastatic lesions in hepatoblastoma. J Pediatr Surg 2007; 42:2050–2056.
56. Ijichi O, Ishikawa S, Shinkoda Y, *et al.* Response of heavily treated and relapsed hepatoblastoma in the transplanted liver to single-agent therapy with irinotecan. Pediatr Transplant 2006; 10:635–638.

Copyright © Lippincott Williams & Wilkins. Unauthorized reproduction of this article is prohibited.

57. Beaty O III, Berg S, Blaney S, *et al.* A phase II trial and pharmacokinetic study of oxaliplatin in children with refractory solid tumors: a Children's Oncology Group study. Pediatr Blood Cancer 2010; 55:440–445.
58. Gray SG, Eriksson T, Ekström C, *et al.* Altered expression of members of the IGF-axis in hepatoblastomas. Br J Cancer 2000; 82:1561–1567.
59. Tomizawa M, Saisho H. Signaling pathway of insulin-like growth factor-II as a target of molecular therapy for hepatoblastoma. World J Gastroenterol 2006; 12:6531–6535.
60. Hartmann W, Küchler J, Koch A, *et al.* Activation of phosphatidylinositol-3′-kinase/AKT signaling is essential in hepatoblastoma survival. Clin Cancer Res 2009; 15:4538–4545.
61. Bjornsti M-A, Houghton PJ. The TOR pathway: a target for cancer therapy. Nat Rev Cancer 2004; 4:335–348.
62. McCrudden KW, Hopkins B, Frischer J, *et al.* Anti-VEGF antibody in experimental hepatoblastoma: suppression of tumor growth and altered angiogenesis. J Pediatr Surg 2003; 38:308–314; discussion 308–314.
63. Warmann SW, Fuchs J, Bitzer M, *et al.* Emerging gene-directed antitumor strategies against human hepatoblastoma. Expert Opin Biol Ther 2009; 9:1155–1161.
64. Lieber J, Kirchner B, Eicher C, *et al.* Inhibition of Bcl-2 and Bcl-X enhances chemotherapy sensitivity in hepatoblastoma cells. Pediatr Blood Cancer 2010; 55:1089–1095.
65. Jacobs JFM, Coulie PG, Figdor CG, *et al.* Targets for active immunotherapy against pediatric solid tumors. Cancer Immunol Immunother 2009; 58:831–841.

Copyright © Lippincott Williams & Wilkins. Unauthorized reproduction of this article is prohibited.

OPEN ACCESS Freely available online

PLOS | GENETICS

NCYM, a *Cis*-Antisense Gene of *MYCN*, Encodes a *De Novo* Evolved Protein That Inhibits GSK3β Resulting in the Stabilization of MYCN in Human Neuroblastomas

Yusuke Suenaga[1], S. M. Rafiqul Islam[1], Jennifer Alagu[1], Yoshiki Kaneko[1], Mamoru Kato[2], Yukichi Tanaka[3], Hidetada Kawana[4], Shamim Hossain[1¤a], Daisuke Matsumoto[1], Mami Yamamoto[1], Wataru Shoji[1,5], Makiko Itami[4], Tatsuhiro Shibata[2], Yohko Nakamura[1], Miki Ohira[6], Seiki Haraguchi[1¤b], Atsushi Takatori[1], Akira Nakagawara[1]*

1 Division of Biochemistry and Innovative Cancer Therapeutics and Children's Cancer Research Center, Chiba Cancer Center Research Institute, 666-2 Nitona, Chuo-ku, Chiba, Japan, **2** Division of Cancer Genomics, National Cancer Center Research Institute, 5-1-1 Tsukiji, Chuo-ku, Tokyo, Japan, **3** Department of Diagnostic Pathology, Research Institute, Kanagawa Children's Medical Center, 2-138-4 Mutsukawa, Minami-ku, Yokohama, Japan, **4** Division of Surgical Pathology, Chiba Cancer Center, 666-2 Nitona, Chuo-ku, Chiba, Japan, **5** Department of Pediatric Surgery, Graduate School of Medicine, Tohoku University, Sendai, Japan, **6** Laboratory of Cancer Genomics, Chiba Cancer Center Research Institute, 666-2 Nitona, Chuo-ku, Chiba, Japan

Abstract

The rearrangement of pre-existing genes has long been thought of as the major mode of new gene generation. Recently, *de novo* gene birth from non-genic DNA was found to be an alternative mechanism to generate novel protein-coding genes. However, its functional role in human disease remains largely unknown. Here we show that *NCYM*, a *cis*-antisense gene of the *MYCN* oncogene, initially thought to be a large non-coding RNA, encodes a *de novo* evolved protein regulating the pathogenesis of human cancers, particularly neuroblastoma. The *NCYM* gene is evolutionally conserved only in the taxonomic group containing humans and chimpanzees. In primary human neuroblastomas, *NCYM* is 100% co-amplified and co-expressed with *MYCN*, and *NCYM* mRNA expression is associated with poor clinical outcome. MYCN directly transactivates both *NCYM* and *MYCN* mRNA, whereas NCYM stabilizes MYCN protein by inhibiting the activity of GSK3β, a kinase that promotes MYCN degradation. In contrast to *MYCN* transgenic mice, neuroblastomas in *MYCN/NCYM* double transgenic mice were frequently accompanied by distant metastases, behavior reminiscent of human neuroblastomas with *MYCN* amplification. The NCYM protein also interacts with GSK3β, thereby stabilizing the MYCN protein in the tumors of the *MYCN/NCYM* double transgenic mice. Thus, these results suggest that GSK3β inhibition by NCYM stabilizes the MYCN protein both *in vitro* and *in vivo*. Furthermore, the survival of *MYCN* transgenic mice bearing neuroblastoma was improved by treatment with NVP-BEZ235, a dual PI3K/mTOR inhibitor shown to destabilize MYCN via GSK3β activation. In contrast, tumors caused in *MYCN/NCYM* double transgenic mice showed chemo-resistance to the drug. Collectively, our results show that NCYM is the first *de novo* evolved protein known to act as an oncopromoting factor in human cancer, and suggest that *de novo* evolved proteins may functionally characterize human disease.

Citation: Suenaga Y, Islam SMR, Alagu J, Kaneko Y, Kato M, et al. (2014) *NCYM*, a *Cis*-Antisense Gene of *MYCN*, Encodes a *De Novo* Evolved Protein That Inhibits GSK3β Resulting in the Stabilization of MYCN in Human Neuroblastomas. PLoS Genet 10(1): e1003996. doi:10.1371/journal.pgen.1003996

Editor: Martin Eilers, Universität Würzburg, Germany

Received April 18, 2013; **Accepted** October 18, 2013; **Published** January 2, 2014

Copyright: © 2014 Suenaga et al. This is an open-access article distributed under the terms of the Creative Commons Attribution License, which permits unrestricted use, distribution, and reproduction in any medium, provided the original author and source are credited.

Funding: This work was supported in part by a Grant-in-Aid from the Ministry of Health, Labour and Welfare for the Third Term Comprehensive Control Research for Cancer, Japan (AN), a Grant-in-Aid for Scientific Research on Priority Areas (JSPS KAKENHI Grant Number 17015046) (AN), a Grant-in-Aid for Scientific Research (A) (JSPS KAKENHI Grant Number 24249061) (AN), a Grant-in-Aid for Research Activity start-up (JSPS KAKENHI Grant Number 22890241) (YS) and a Grant-in-Aid for Young Scientists (B) (JSPS KAKENHI Grant Number 24700957) (YS) from the Japan Society for the Promotion of Science (JSPS), a Global COE program (Global Center for Education and Research in Immune System Regulation and Treatment), Graduate School of Medicine, Chiba University (AN and YS), Takeda Science Foundation (AN), and National Cancer Center Research and Development Fund (23-A-8) (TS). The funders had no role in study design, data collection and analysis, decision to publish, or preparation of the manuscript.

Competing Interests: The authors have declared that no competing interests exist.

* E-mail: akiranak@chiba-cc.jp

¤a Current address: Department of Integrative Physiology, Graduate School of Medical Sciences, Kyushu University, 3-1-1 Maidashi, Higashi-ku, Fukuoka, Japan. ¤b Current address: Animal Breeding and Reproduction Division, NARO Institute of Livestock and Grassland Science, 2 Ikenodai, Tsukuba, Japan.

Introduction

Gene evolution has long been thought to arise from pre-existing genes through duplication or rearrangement followed by rapid divergence [1–5]. *De novo* gene birth from non-coding genomic regions has been generally believed to be exceptionally rare [1]. However, recent studies using genome-wide analyses have suggested the presence of a large number of *de novo* evolved genes in some species [3,5–11], including primates [12–17]. Studies in yeast revealed that the proteins produced from *de novo* genes were not insignificant polypeptides but functional proteins [6,7] and that *de novo* gene birth could be a major mechanism of new gene generation [6]. In multicellular organisms, however, the functions of *de novo* evolved proteins have been poorly characterized [3,15], and thus their pathophysiological significance has remained elusive. Therefore, it is still unclear whether *de novo* gene birth is a general mechanism throughout evolution for the creation of functional protein-coding genes.

Author Summary

The *MYCN* oncogene has a central role in the genesis and progression of neuroblastomas, and its amplification is associated with an unfavorable prognosis. We have found that *NCYM*, a *MYCN cis*-antisense RNA, is translated in humans to a *de novo* evolved protein. NCYM inhibits GSK3β to stabilize MYCN, whereas MYCN induces *NCYM* transcription. The positive feedback regulation formed in the *MYCN/NCYM*-amplified tumors promotes the aggressive nature of human neuroblastoma. *MYCN* transgenic mice, which express human *MYCN* in sympathoadrenal tissues, spontaneously develop neuroblastomas. However, unlike human neuroblastoma, distant metastasis is infrequent. We established *MYCN/NCYM* double transgenic mice as a new animal model for studying neuroblastoma pathogenesis. We found that NCYM expression promoted both the metastasis and chemo-resistance of the neuroblastomas formed in the double transgenic mice. These results demonstrate that NCYM may be a potential target for developing novel therapeutic tools against high-risk neuroblastomas in humans, and that the *MYCN/NCYM* double transgenic mouse may be a suitable model for the screening of these new drugs.

Neuroblastoma is one of the most common solid tumors in children. It originates from the neuronal precursor cells of the sympathoadrenal lineage of the neural crest [18]. Its clinical behavior is enigmatic; the tumors in patients of less than one year of age often regress spontaneously, whereas the tumors detected in patients over one year of age are usually aggressive and eventually cause the patient's death despite intensive multimodality therapies [18]. The *MYCN* oncogene is frequently amplified in those tumors that occur in patients who are over one year of age at diagnosis [19,20]. Transgenic mice expressing human *MYCN* in sympathoadrenal tissues spontaneously develop neuroblastomas [21], suggesting that *MYCN* alone can initiate tumorigenesis and promote tumor growth. However, unlike human neuroblastoma, its distant metastasis is infrequent. Furthermore, in human neuroblastomas without *MYCN* amplification, *MYCN* mRNA expression levels do not correlate with the prognosis of the patients [22,23], suggesting that additional events might contribute to the acquisition of increased aggressiveness. We focused on *NCYM* as a candidate gene that promotes the aggressiveness of *MYCN*-amplified neuroblastomas. *NCYM* is a *cis*-antisense gene of *MYCN* [24,25] and is co-amplified with *MYCN* in human neuroblastoma cells. *NCYM* is transcribed in the opposite direction to *MYCN*, starting from intron 1 of the *MYCN* gene (Figure 1A), and it has remained unclear for a long time whether the gene encodes a functional protein [24,26]. In this study, we have found that NCYM is indeed a functional protein that regulates MYCN function in human, but not mouse, neuroblastoma.

Results

NCYM is a *de novo* evolved gene

We first analyzed the genomic sequence of *NCYM* in various species and found that in humans and chimpanzees the potential NCYM protein is composed of 109 amino acids (Figure 1B, Figure S1). We next searched for paralogs and orthologs of the human NCYM protein among other animals using the Basic Local Alignment Search Tool (BLAST) databases with an E-value threshold of 10^{-3}. We did not find any paralogs, but identified orthologs for a probable NCYM protein in olive baboons, chimpanzees and pigmy chimpanzees. From here on, we focused on the *NCYM* gene of the hominidae to investigate the function of the protein product. The evolutionary rates between the indicated species suggest that the coding sequence of *NCYM* gene was exposed to positive selection in humans and chimpanzees (Figure 1C), and the amino acid frequencies in these species were significantly different from the uniform usage of amino acids ($P<0.001$; Figure S2). We next raised an antibody against the putative human NCYM protein, and identified a 12 to 15 kDa protein in human neuroblastoma cells which mainly localized to nuclei in *MYCN*-amplified neuroblastoma cells (Figure S3, Figure S4). The NCYM protein was expressed in a variety of normal human tissues, including the neuronal cells of the cerebrum and cerebellum, spermatocytes of the testis, pancreatic cells and also the heart (Figure S5). NCYM was also localized in both the nucleus and cytoplasm in these cells (Figure S5A–D). NCYM was expressed in both primary and metastatic human neuroblastomas (Figure 1D, Figure S5E and F), and was co-expressed with the MYCN protein in cells of human neuroblastomas (Figure 1D and E) and the neuronal cells of the human cerebrum (Figure 1F and G). It was also co-expressed with the MYCN protein in some primary human cancers, including thyroid cancer (Figure S6). Thus, the NCYM protein is a *de novo* evolved gene product and is endogenously expressed in both normal human tissues and cancers.

Prognostic significance of *NCYM* expression in human neuroblastoma

We next examined the prognostic significance of *NCYM* mRNA expression in human neuroblastoma. The *NCYM* gene was co-amplified with the *MYCN* gene in all the cell lines and primary neuroblastomas we examined (Figure S7). *NCYM* expression levels were significantly correlated with that of *MYCN* in primary neuroblastomas ($n=106$, $P=4.69\times10^{-16}$; Figure 2A) and in the tumors with a single copy of *MYCN* ($n=86$, $P=1.11\times10^{-13}$; Figure 2B). In addition, high levels of *NCYM* mRNA expression were significantly associated with unfavorable prognostic factors ($P<0.05$, Table S1) and a poor outcome ($P=3.70\times10^{-5}$; Figure 2C), similar to that for *MYCN* mRNA expression ($P<0.05$; Table S1 and $P=2.31\times10^{-5}$; Figure 2D). Interestingly, high levels of *NCYM* mRNA expression were also significantly correlated with poor outcome in those patients diagnosed at over one year of age without *MYCN* amplification ($n=45$, $P=0.0375$; Figure S8A) whereas those of *MYCN* did not correlate with the prognoses ($n=45$, $P=0.144$; Figure S8B). Multivariate analysis of 106 primary neuroblastomas showed, as expected, that *NCYM* mRNA expression is not an independent prognostic factor from expression and amplification of *MYCN* (Table S2). However, it is an independent prognostic factor from age at diagnosis, stage and *TrkA* expression.

Positive feedback regulation between NCYM and MYCN

The co-amplification and co-expression of *NCYM* and *MYCN* in human primary neuroblastomas prompted us to investigate the functional interaction between NCYM and MYCN. Previously we have reported that MYCN directly targets its own expression in neuroblastoma cell lines [27]. Because the promoter region of the *NCYM* gene is localized within intron 1 of *MYCN* (Figure S9A), we examined whether MYCN regulates *NCYM* transcription. Overexpression of MYCN in human neuroblastoma cells induced *NCYM* mRNA expression (Figure 3A), whereas shRNA-mediated knockdown of *MYCN* downregulated endogenous *NCYM* mRNA levels (Figure 3B). MYC overexpression did not induce either *MYCN* or *NCYM* expression (Figure S9B). However, MYCN

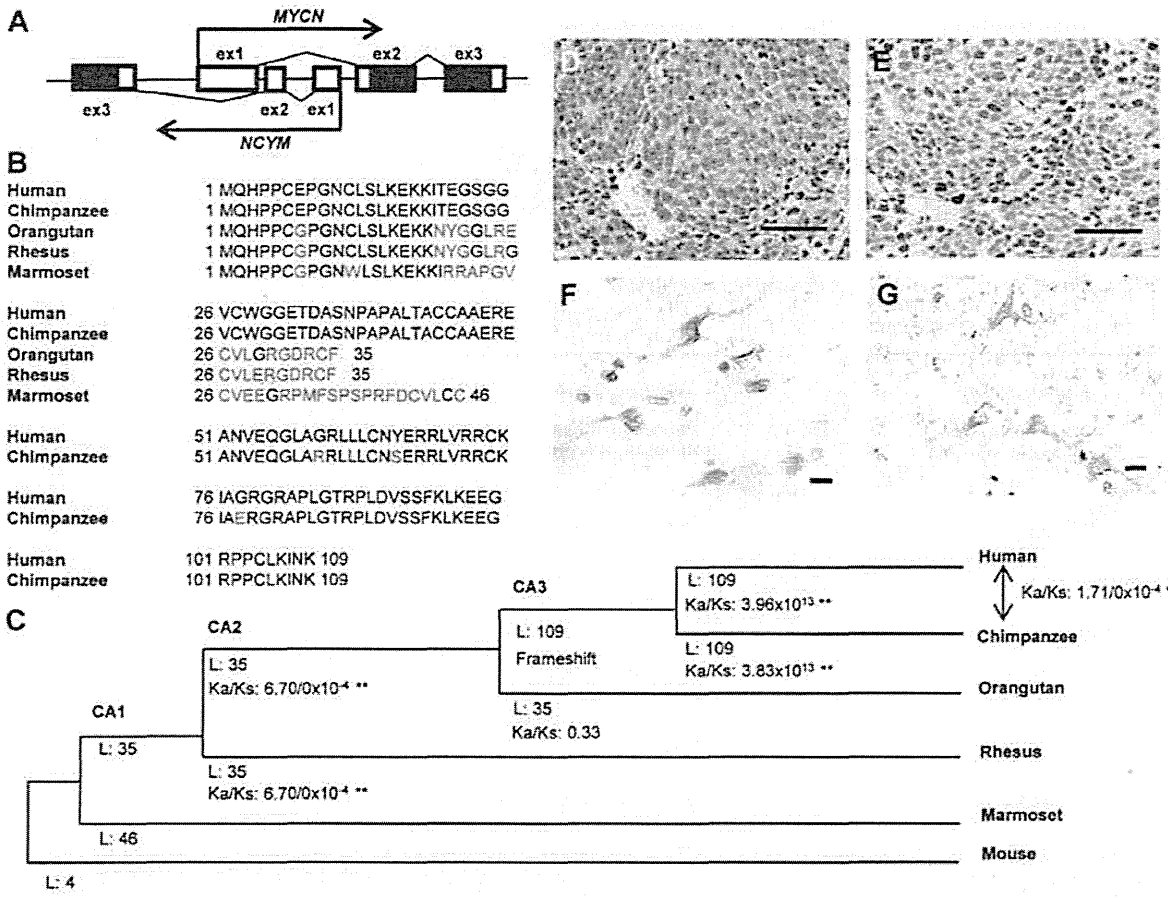

Figure 1. *NCYM* encodes a *de novo* evolved protein in humans. (A) Gene structure of the human *MYCN/NCYM* locus. (B) Alignment of the possible amino acid sequences of NCYM in the human and primate genomes, where the ORF of the primate genes begins at the same position as the human start codon. Red text indicates amino acid differences compared with human NCYM. (C) Change in protein features along the lineage shown. CA indicates common ancestor. L indicates the sequence length of amino acids before the first terminal codon. Asterisk indicates statistical significance (**$P<0.001$, *$P<0.05$). K_a and K_s indicate the rate of non-synonymous changes and synonymous changes, respectively. (D–G) The protein expression of NCYM and MYCN in human primary neuroblastomas (D, E) and normal human cerebrum (F, G). Scale bars, 100 μm (D, E) and 50 μm (F, G). Sections of neuroblastomas with *MYCN* amplification and those of normal human cerebrum were stained with anti-NCYM (D, F) or anti-MYCN (E, G) antibodies.
doi:10.1371/journal.pgen.1003996.g001

overexpression did enhance *NCYM* promoter activity in a dose-dependent manner (Figure 3C), suggesting that MYCN, but not MYC, activates the transcription of *NCYM*. Putative E-boxes exist in intron 1 of the *MYCN* gene; however, it is unclear whether they are responsible for this feedback regulation. We therefore generated constructs containing different lengths of the MYCN intron 1 region and performed luciferase assays to identify the MYCN-responsive region (Figure S9C). MYCN enhances its own promoter activity in a dose-dependent manner when co-transfected with reporter plasmids containing the NCYM promoter region (from +1073 to +1312). However, when co-transfected with plasmids without this NCYM promoter region, MYCN positive autoregulation was diminished. Within this region, there is a putative E-box located just 2 base pairs upstream from the transcription start site of the *NCYM* gene (Figure S10A). We generated constructs containing the NCYM promoter region comprising either a wild-type or a mutant E-box. Overexpression of MYCN enhanced NCYM wild-type promoter activity, but mutation of the E-box diminished its activation (Figure S10C). MYC overexpression did not activate either of the NCYM promoter constructs (Figure S10B and C). Therefore, these results indicate that MYCN enhances NCYM promoter activity in an E-box-dependent manner. MYC, however, is not involved in *NCYM* transcription.

We next investigated the function of NCYM in neuroblastoma cells. NCYM overexpression induced MYCN protein levels (Figure 3D, left panel; Figure S11A), but had no effect on the mRNA levels of *MYCN* (Figure 3D, right panel; Figure S11A). Consistent with these results, shRNA-mediated knockdown of NCYM significantly downregulated the amount of MYCN protein without affecting the level of *MYCN* mRNA expression (Figure 3E). In addition, knockdown of NCYM decreased the stability of the MYCN protein (Figure S11B). This NCYM knockdown-mediated destabilization of MYCN could be inhibited using the proteasome inhibitor MG132 (Figure S11C). It is known that the stability of the MYCN protein is regulated by a series of phosphorylation and ubiquitination events that are required for its recognition by the proteasome [28]. CDK1/Cyclin B1 phosphorylates MYCN at serine 62: the mono-phosphorylated MYCN is then recognized by GSK3β and subsequently phosphorylated at threonine 58, leading